



Contents lists available at ScienceDirect

Journal of Sound and Vibration

journal homepage: www.elsevier.com/locate/jsvi

Delayed resonator with multiple distributed delays – Considering and optimizing the inherent loop delay

Yifan Liu ^a, Nejat Olgac ^b, Li Cheng ^{a,*}^a Department of Mechanical Engineering, The Hong Kong Polytechnic University, Kowloon, Hong Kong, China^b Department of Mechanical Engineering, University of Connecticut, Storrs, CT, USA

ARTICLE INFO

Keywords:

Active vibration control
 Delayed resonator
 Multiple-delay distributed-delay system

ABSTRACT

We generalize the distributed delayed resonator (DDR) concept by incorporating the previously unutilized but inevitable feedback loop delay, thus creating a so-called multiple-delay distributed delayed resonator (MD-DDR) for complete vibration suppression. The necessary parameter tuning and control stability analysis become more involved but remain analytically solvable. Particularly, we take the operability of control parameters imposed by hardware as an explicit condition for parameter tuning and show that the loop delay (even if it is small) can lead to incomplete vibration suppression and, counter-intuitively, even no suppression if the excitation frequency exceeds a threshold value. On the other hand, such negative effects are neutralized by correcting control parameters. The loop delay is then intentionally augmented to seek enhanced performance, yielding a considerably extended operable frequency band for the desired complete vibration suppression. Furthermore, it is optimized to expedite response speed by achieving the leftmost placement of the dominant (i.e., the rightmost) characteristic root. Instead of applying a brute-force sweeping procedure as in the previous works, we analyze the dominant root locus and seek if the jump phenomenon occurs to conduct exact optimization at a low computational cost. Finally, extensive comparisons using actual experimental parameters are performed to explore various effects of the loop delay on vibration suppression and the benefits of the proposed MD-DDR in handling such issues over the conventional DDR that treats a single delay. This study fully exploits the strength of the distributed delayed control logic, moving the DDR concept closer to real applications and aiming to establish a broader design and analysis framework for the delayed resonator from a multiple-delay perspective.

1. Introduction

Vibration control is vital to avoid consequences such as material fatigue and structural damage. We are interested in the concept of dynamic vibration absorber (DVA). The original DVA comprising a mass and a linear spring was invented in the 1900s by Frahm [1] to interact with the primary structure to achieve complete vibration suppression only at its natural frequency. Den Hartog and Ormondroyd [2] later injected a damper into the DVA yielding broadband vibration reduction, which, however, compromised incomplete vibration suppression. To overcome the limitations of passive DVAs, Olgac and his colleagues [3] introduced the concept of delayed resonator (DR) in 1994 by using delayed feedback actuation to drive DVAs so that vibrations even at a time-varying frequency

* Corresponding author:

E-mail address: li.cheng@polyu.edu.hk (L. Cheng).

<https://doi.org/10.1016/j.jsv.2024.118290>

Received 28 June 2023; Received in revised form 11 January 2024; Accepted 17 January 2024

Available online 20 January 2024

0022-460X/© 2024 Elsevier Ltd. All rights reserved.

can be fully suppressed by tuning the gain and the delay parameters in real-time.

Modifications to the DR technique have never ceased since its invention. Earlier DR investigations focused on the feedback design using different resonator states, e.g., displacement [1] and acceleration [4]. Nowadays, the DR concept has been developed in various fields. For instance, Kim and Brennan [5] used delayed resonant feedback to suppress multiple vibration modes. Nia and Sipahi [6] designed a robust controller to handle delay disturbances. Zhang et al. [7] deployed the DR to reduce vibrations on a vehicle seat suspension, see also [8] for optimal control. Xu and Sun [9,10] reported the identification process of loop delay for a practical DR implementation. More recently, Eris et al. [11] injected an additional non-delayed control term into the control loop to extend the operable frequency band. Pilbauer et al. [12] proposed a polynomial distribution-based logic to handle the mismatches between the actual vibration frequency and the detected one by sensors. Liu et al. [13,14] showed that the delayed control logic can effectively suppress vibrations on micro/nano-electro-mechanical systems. Villa and Aguilar [15] analyzed a DR subsystem actuated by delayed position and velocity terms. Karama et al. [16] attempted to harvest energy while suppressing vibrations by properly sensitizing the DR dynamics. Wang et al. [17] deployed the DR for nonlinear vibration absorption, see also [18–22] for delayed vibration isolation. The DR concept is then generalized to have multiple degrees of freedom to achieve non-collocated vibration absorption [23–27], i.e., the DR location can be different from the complete suppression point. Besides, Vyhřídál et al. [28] compared the behaviors of the DR when the feedback actuation based on different resonator states. Cai et al. [29,30] further established the connection among different states using fractional calculus and showed that tuning fractional order can enhance robustness and transient behaviors, see also [31] for similar enhancement using a mechanical amplifying mechanism. The DR is also modified for multiple-dimensional vibration absorption to simultaneously suppress translational and rotational vibrations [32–34]. We also remark that the delayed control logic is equivalent to tuning the stiffness and damping of the resonator similar to the PD control, while the superiority of the delay-based logic from both software and hardware aspects was discussed in [32]. Besides, properly designing the delayed logic allows suppressing multiple-frequency vibration via a single-mass absorber [35], which is not something that can be achieved by the PD control and other non-delayed control logic.

However, all the above DR investigations entail producing feedback force by directly delaying the signals from the sensor measurements and then amplifying them with a designed gain, which obviously leads to poor performance if the measurements are noisy, and this problem is more serious if numerical derivative is needed. To this end, Pilbauer et al. [36] and Kučera et al. [37] proposed a distributed-type delayed logic so that all sensor measurements within a designed time interval $\bar{t} \in [\bar{t} - \bar{\tau}, \bar{t}]$ were summed up for feedback design, where \bar{t} is present time and $\bar{\tau}$ is the delay. Indeed, the distributed operation suppresses the noise effects as also experimentally verified in the given two references, while the effect of the loop delay, labeled as $\bar{\delta}$ and caused by inevitable operations in the control loop, such as sampling and communicating [38,39], on such a distributed-type control logic has not yet been fully explored since sensor measurements within the time interval $\bar{t} \in [\bar{t} - \bar{\delta}, \bar{t}]$ are not available to the controller at time \bar{t} . Hence, the desired complete suppression is impractical using the single-distributed-delayed logic. On the other hand, most DR studies focus on the single-delay feedback control design, and some studies, such as [18,35], have shown that the multiple-delay-based control logic can yield additional benefits on vibration suppression in both linear and nonlinear fields. Thus, we are also interested in the possible advantages of tactically manipulating $\bar{\delta}$, making it worthwhile to consider the following unexplored questions to bring the distributed-delayed control logic closer to real applications.

A1. How does the blinded interval $[\bar{t} - \bar{\delta}, \bar{t}]$ affect the desired complete suppression when adopting the single-distributed-delayed logic? How to fix it, and how to correct control parameters by considering the multiple-delay effect?

A2. What benefits can be obtained by treating $\bar{\delta}$ as a new control parameter? How to design it?

However, answering such questions is nontrivial, especially given that introducing an additional delay leads to a multiple-delay system, thus greatly complicating the analysis. For Aspect 1 (A1), the half-angle substitution [40] is applied so that parameter tuning and stability issues of the coupled system are both analytically tackled in a non-conservative manner. Note that the stability of the coupled system in previous studies [36,37] was only numerically examined. Furthermore, knowing that the applicability of the DR in the high-frequency band was limited by the unduly small tuned delay [4,28], we formally take it as an explicit condition for the parametric design. For A2, the tunable $\bar{\delta}$ yields an additional control parameter, and its effects on the operable frequency interval for complete vibration suppression and the response speed are mainly considered. We stress that optimizing parameters to expedite responses has been considered in [11,29,31] using a brute-force sweeping method. Instead, a simplified exact procedure is proposed here by analyzing the root locus. At last, numerous comparisons using the parameters of the experimental setup in [36,37] are made to

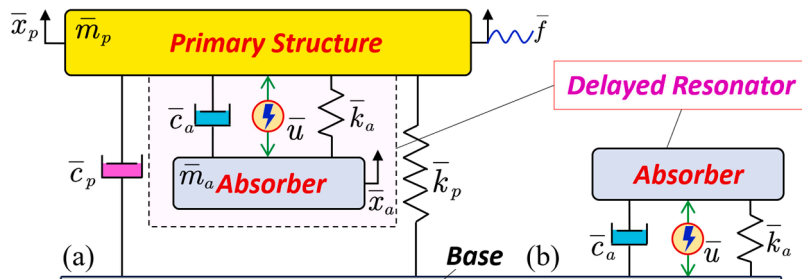


Fig. 1. (a). Schematic model of the DR configuration. (b). Equivalent model of (a) when $\bar{x}_p \equiv 0$.

unveil the possible negative effects of $\bar{\delta}$ and the significant benefits that can be obtained by properly tuning $\bar{\delta}$. These milestones extend the DR knowledge from both theoretical and practical aspects.

This paper is structured as follows. Section 2 reviews the DR concept and establishes the general dynamic model. Sections 3 and 4 determine and analyze the tuned parameters, respectively. Stability issues are analytically tackled in Section 5. Section 6 introduces the parameter optimization procedure to expedite the transient process. Section 7 presents four elaborate simulations. Section 8 draws conclusions. Italic symbols without the bar superscript $\bar{\square}$ are dimensionless throughout the text.

2. Preliminaries

A common operating mode of the DR is shown in Fig. 1(a), where a feedback actuation \bar{u} based on the actively delayed absorber states is injected into a 2-degree-of-freedom (2DOF) coupled system. The aim is to properly design the delayed feedback actuation \bar{u} so that vibrations on the primary structure excited by a harmonic force \bar{f} can be completely suppressed. When this is achieved, the primary structure is equivalent to a fictitious ground, and the coupled system behaves like Fig. 1(b).

2.1. General mathematical model

Dynamics of the coupled system shown in Fig. 1(a) have been widely considered in the previous DR studies. The only variable is the form of the delayed feedback actuation \bar{u} . To this end, we establish the general system dynamics. The governing equations of the coupled system are

$$\begin{bmatrix} \bar{m}_p & 0 \\ 0 & \bar{m}_a \end{bmatrix} \begin{bmatrix} \ddot{\bar{x}}_p \\ \ddot{\bar{x}}_a \end{bmatrix} + \begin{bmatrix} \bar{c}_p + \bar{c}_a & -\bar{c}_a \\ -\bar{c}_a & \bar{c}_a \end{bmatrix} \begin{bmatrix} \dot{\bar{x}}_p \\ \dot{\bar{x}}_a \end{bmatrix} + \begin{bmatrix} \bar{k}_p + \bar{k}_a & -\bar{k}_a \\ -\bar{k}_a & \bar{k}_a \end{bmatrix} \begin{bmatrix} \bar{x}_p \\ \bar{x}_a \end{bmatrix} = \begin{bmatrix} \bar{f} - \bar{u} \\ \bar{u} \end{bmatrix}, \tag{1}$$

where the subscripts $(\cdot)_p$ and $(\cdot)_a$ denote the primary structure and absorber, respectively; and the notations $\bar{x}_{(\cdot)}$, $\bar{m}_{(\cdot)}$, $\bar{c}_{(\cdot)}$, and $\bar{k}_{(\cdot)}$ represent the displacement, mass, damping, and stiffness, respectively. Moreover, $\bar{x}_{(\cdot)}$, \bar{u} , and \bar{f} are all functions of the physical time \bar{t} . The feedback actuation \bar{u} based on the linear delayed absorber states is expressed as

$$\mathcal{L}(\bar{u}) = \bar{U}(\bar{s}, e^{-\bar{\tau}\bar{s}})X_a, \tag{2}$$

where \bar{s} is the Laplace variable, $\bar{\tau}$ is the delay, \bar{U} is a quasi-polynomial in $(\bar{s}, e^{-\bar{\tau}\bar{s}})$, and $\mathcal{L}(\cdot)$ represents the Laplace transformation operation such that $X_a = \mathcal{L}(\bar{x}_a)$. Then, the governing equation (1) in the Laplace domain is

$$\begin{bmatrix} \bar{m}_p \bar{s}^2 + (\bar{c}_p + \bar{c}_a)\bar{s} + \bar{k}_p + \bar{k}_a & -(\bar{c}_a \bar{s} + \bar{k}_a) + \bar{U}(\bar{s}, e^{-\bar{\tau}\bar{s}}) \\ -(\bar{c}_a \bar{s} + \bar{k}_a) & \bar{m}_a \bar{s}^2 + \bar{c}_a \bar{s} + \bar{k}_a - \bar{U}(\bar{s}, e^{-\bar{\tau}\bar{s}}) \end{bmatrix} \begin{bmatrix} X_p \\ X_a \end{bmatrix} = \begin{bmatrix} F \\ 0 \end{bmatrix}, \tag{3}$$

in which $X_p = \mathcal{L}(\bar{x}_p)$ and $F = \mathcal{L}(\bar{f})$. Introducing the following scaled variables

$$\begin{aligned} \bar{\omega}_p &= \sqrt{\frac{\bar{k}_p}{\bar{m}_p}}, \bar{\omega}_a = \sqrt{\frac{\bar{k}_a}{\bar{m}_a}}, \zeta_p = \frac{\bar{c}_p}{(2\bar{m}_p \bar{\omega}_p)}, \zeta_a = \frac{\bar{c}_a}{(2\bar{m}_a \bar{\omega}_a)}, \mu = \frac{\bar{m}_a}{\bar{m}_p}, \nu = \frac{\bar{\omega}_a}{\bar{\omega}_p}, \\ s &= \bar{s} / \bar{\omega}_p, \tau = \bar{\tau} \bar{\omega}_p, U(s, e^{-\tau s}) = \bar{U} / (\bar{m}_p \bar{\omega}_p^2), \end{aligned} \tag{4}$$

into (3) yields the dimensionless governing equation in a matrix form of

$$\mathbf{M}\mathbf{X} = \mathbf{F}, \tag{5}$$

where $\mathbf{X} = [X_p, X_a]^T$, $\mathbf{F} = [F/\bar{k}_p, 0]^T$, and

$$\mathbf{M} = \begin{bmatrix} s^2 + 2\zeta_p s + 1 + \mu\nu(2\zeta_a s + \nu) & -\mu\nu(2\zeta_a s + \nu) + U(s, e^{-\tau s}) \\ -\mu\nu(2\zeta_a s + \nu) & \mu(s^2 + 2\zeta_a \nu s + \nu^2) - U(s, e^{-\tau s}) \end{bmatrix}. \tag{6}$$

We can then obtain the transfer function between the displacement \bar{x}_p of the primary structure and the excitation force \bar{f}

$$G(s, U) = \frac{X_p}{F/\bar{k}_p} = \mathbf{M}_{(1,1)}^{-1} = \frac{N(s, U)}{CE(s, U)}, \tag{7}$$

where $\mathbf{M}_{(1,1)}^{-1}$ represents the (1, 1) element of the matrix \mathbf{M}^{-1} , and

$$\begin{cases} N(s, U) = \mu(s^2 + 2\zeta_a \nu s + \nu^2) - U(s, e^{-\tau s}), \\ CE(s, U) = (s^2 + 2\zeta_p s + 1)(\mu(s^2 + 2\zeta_a \nu s + \nu^2) - U) + \mu^2 s^2 \nu(2\zeta_a s + \nu). \end{cases} \tag{8}$$

Consequently, the characteristic equation of the coupled system is

$$CE(s, U) = 0. \tag{9}$$

Clearly, the spectrum of Eq. (9) must lie on the left half of the complex plane for stability.

2.2. Distributed delayed control logic

The delayed feedback actuation \bar{u} is designed to completely suppress the vibrations on the primary structure at a given frequency, say $\bar{\omega} \in \mathbb{R}^+$. That is, we require $|G(s = j\omega)| \equiv 0$, where $\omega = \bar{\omega}/\bar{\omega}_p, j = \sqrt{-1}$, yielding

$$N(s = j\omega, U) = \mu(v^2 - \omega^2) + j2\zeta_a\mu v\omega - U(s, e^{-\tau s})_{s=j\omega} \equiv 0. \tag{10}$$

The form of the function $U(s, e^{-\tau s})$ dictates the vibration suppression performance. Existing investigations focus more on the single-delay tuning mechanism, exemplified by the following two acceleration-based control logics

$$\begin{cases} \bar{u}_{SL}(\bar{t}, \bar{g}, \bar{\tau}) = \bar{g}\ddot{\bar{x}}_a(\bar{t} - \bar{\tau}), \\ \bar{u}_{SD}(\bar{t}, \bar{g}, \bar{\tau}) = \bar{g}\frac{1}{\bar{\tau}} \int_0^{\bar{\tau}} \ddot{\bar{x}}_a(\bar{t} - \bar{\theta})d\bar{\theta}, \end{cases} \tag{11}$$

where \bar{g} is an auxiliary symbol denoting the gain. The logic \bar{u}_{SL} and \bar{u}_{SD} is known as lumped [4] and distributed type [36,37], respectively. Clearly, the latter type \bar{u}_{SD} performs better, especially when the acceleration measurements are noisy thanks to the integral operation, which functions as a moving average filter. However, the lower limit of the integral operation being zero ignores the inevitable loop delays, and instead, a more practical distributed-type logic should be

$$\bar{u}_{MD}(\bar{t}, \bar{g}, \bar{\tau}_1, \bar{\tau}_2) = \bar{g} \int_{\bar{\tau}_2}^{\bar{\tau}_1} \ddot{\bar{x}}_a(\bar{t} - \bar{\theta})d\bar{\theta}, \bar{\tau}_1 > \bar{\tau}_2 \geq \bar{\delta} > 0, \tag{12}$$

where $\bar{g} = \bar{g}/(\bar{\tau}_1 - \bar{\tau}_2)$, and $\bar{\delta}$ is the smallest inevitable loop delay due to necessary operations such as sampling, calculating, etc. The newly introduced delay $\bar{\tau}_2$ in \bar{u}_{MD} compared with \bar{u}_{SD} takes the hardware delay into account for one thing, and for the other, it can be treated as an additional tunable parameter to seek performance enhancement. With \bar{u}_{MD} , the feedback force is governed by all the absorber states from the time instance $\bar{t} - \bar{\tau}_1$ to $\bar{t} - \bar{\tau}_2$, see Appendix A. Furthermore, we have

$$\mathcal{L}(\bar{u}_{MD}) = \bar{U}_{MD}X_a, \tag{13}$$

where \bar{U}_{MD} according to Eq. (4) has the dimensionless form of

$$U_{MD}(s, g, \tau_1, \tau_2) = g \frac{e^{-\tau_2 s} - e^{-\tau_1 s}}{s} s^2 = gs(e^{-\tau_2 s} - e^{-\tau_1 s}), \tag{14}$$

with the three dimensionless control parameters governed by

$$g = \bar{g}/(\bar{m}_p\bar{\omega}_p), \tau_{1,2} = \bar{\tau}_{1,2}\bar{\omega}_p. \tag{15}$$

Note that the inverse Laplace transform (i.e., time-domain expression) of Eq. (13) can also be expressed as

$$\bar{u}_V(\bar{t}, \bar{g}, \bar{\tau}_1, \bar{\tau}_2) = \bar{g}(\dot{\bar{x}}_a(\bar{t} - \bar{\tau}_2) - \dot{\bar{x}}_a(\bar{t} - \bar{\tau}_1)), \tag{16}$$

which is based on pure velocity. Note, however, that apart from the lumped feedback type, the increased number of control terms of the logic Eq. (16) compared to Eq. (12) raises robustness concerns. On the other hand, we can find from the forms of Eqs. (11)-(16) that the resulting neutral-type delayed system when adopting \bar{u}_L reduces to the retarded type by deploying \bar{u}_{SD} or \bar{u}_{MD} instead, thus relaxing stability issues [37], an additional benefit of the integral operation beyond filtering noises. Furthermore, plugging Eq. (14) into Eq. (10) gives

$$N(\omega, g, \tau_1, \tau_2) = \mu(v^2 - \omega^2) + j2\zeta_a\mu v\omega + jg\omega(e^{-j\tau_1\omega} - e^{-j\tau_2\omega}) = 0. \tag{17}$$

Consequently, one main objective of the controller design is to tune the parameter composition $(\omega, g, \tau_1, \tau_2)$ according to Eq. (17). Moreover, substituting (13) into (8) leads to the characteristic equation of the resonator subsystem

$$N(s, g, \tau_1, \tau_2) = \mu(s^2 + 2\zeta_a vs + v^2) + gs(e^{-\tau_1 s} - e^{-\tau_2 s}) = 0, \tag{18}$$

which holds as if the resonator is mounted on the ground, see Fig. 1(b). Similarly, we have

$$CE(s, g, \tau_1, \tau_2) = (s^2 + 2\zeta_p s + 1)(\mu(s^2 + 2\zeta_a vs + v^2) - gs(e^{-\tau_2 s} - e^{-\tau_1 s})) + \mu^2 s^2 v(2\zeta_a s + v) = 0 \tag{19}$$

for the coupled system. For discrimination, the two abbreviations SD-DDR and MD-DDR are now used to refer to the single-delay and

multiple-delay distributed delayed resonator, respectively.

3. Tuning mechanism

Tuning the parameter composition (g, τ_1, τ_2) for a variable ω value as per Eq. (17) is the first step of the feedback actuation design for the resonator to completely suppress the vibration at the frequency ω . Besides, the superscripts $(\cdot)^{[1]}$ and $(\cdot)^{[2]}$ in what follows are used to denote the tuned control parameters of the SD-DDR and the MD-DDR, respectively.

3.1. Case 1: Tuned parameter pair (g, τ_1) with $\tau_1 > 0, \tau_2 \rightarrow 0$

Let us first consider the reduced case where the delay τ_2 is ignored, and we are then back to the SD-DDR case. The control parameters to be tuned are the gain g and the delay τ_1 . The corresponding tuning mechanism has been established in [36] and is briefly reviewed in Theorem 1 for comparisons with that of the considered MD-DDR.

Theorem 1. For the SD-DDR to ideally suppress the vibrations at the frequency ω , the parameter pair (g, τ_1) are tuned by

$$\begin{cases} g^{[1]} = \frac{\mu(v^2 - \omega^2)^2}{4\zeta_a v \omega^2} + \zeta_a \mu v, \\ \tau_{1,k}^{[1]} = \frac{2}{\omega} \left[\text{atan2} \left(\frac{2\zeta_a v \omega}{\omega^2 - v^2} \right) + (k - 1)\pi \right], \end{cases} \quad (20)$$

where $k = 1, 2, \dots$ is called branch number, and $\text{atan2}(\cdot) \in [-\pi, \pi]$ denotes the four-quadrant inverse tangent [41].

Proof. Letting $\tau_2 = 0$, Eq. (17) reduces to

$$\mu(v^2 - \omega^2) + j\omega(2\zeta_a \mu v - g) = -jg\omega e^{-j\tau_1 \omega}. \quad (21)$$

The magnitude of the two sides of Eq. (21) should equal yielding

$$\mu^2(v^2 - \omega^2)^2 + (2\zeta_a \mu v \omega - g\omega)^2 = (g\omega)^2, \quad (22)$$

which leads to the tuned gain $g^{[1]}$. Substituting $g = g^{[1]}$ into (21), the argument condition of the resulting new equation yields the tuned delay $\tau_{1,k}^{[1]}$. In particular, the branch number k results from the periodicity of the complex exponent $e^{-j\omega} = e^{-j\omega \pm j2k\pi}$, and the four-quadrant inverse tangent $\text{atan2}(\cdot)$ is used to match the argument of the complex exponent $e^{-j\tau\omega}$. \square

Remark 1. The condition $\text{sgn}(\text{atan2}(Y/X)) = \text{sgn}(Y)$, $X, Y \in \mathbb{R}^2$ always holds for the four-quadrant inverse tangent when tuning the delay. This property determines the selection of the branch number k and the behaviors of the tuned parameters of the MD-DDR. For the former, we can conclude that $k = 1$ corresponds to the smallest positive tuned delay since $2\zeta_a v \omega > 0$, i.e., $0 < \tau_{1,1}^{[1]} < \tau_{1,k+1}^{[1]}$ holds for any frequency ω . Discussions for the latter are performed in Section 4. \square

Remark 2. Two aspects should be noticed from the form of Eq. (20). (i). Given a coupled system, one frequency ω corresponds to a single-valued tuned gain $g^{[1]}$ while the tuned delay $\tau_{1,k}^{[1]}$ can be multi-valued due to the optional branch number k , an exclusive feature of the delayed control logic compared with the PD control for complete vibration absorption. (ii). The tuned gain $g^{[1]} > 0$ of the SD-DDR is always positive. Otherwise, Eq. (22) offers no solutions, meaning that no imaginary roots of Eq. (18) exist, and thus no resonance of the SD-DDR can occur for complete vibration absorption. \square

Corollary 1. For a given coupled system and a branch number k , the tuned delay $\tau_{1,k}^{[1]}$ decreases as the frequency ω increases.

Proof. By inspecting that

$$\frac{\partial \tau_{1,k}^{[1]}}{\partial \omega} = \frac{\tau_{1,k}^{[1]}}{\omega} - \frac{4v\zeta_a(\omega^2 + v^2)}{\omega[(\omega^2 - v^2)^2 + 4\zeta_a^2 \omega^2 v^2]}, \quad (23)$$

we have $\partial \tau_{1,k}^{[1]} / \partial \omega < 0$ when $\omega > 0$. Combining with the condition $\tau_{1,k}^{[1]} > 0$, the proof is completed. \square

3.2. Case 2: Tuned parameter pair (g, τ_1) with $\tau_1 > 0, \tau_2 > 0$

The aim is to determine the composition (ω, g, τ_1) satisfying Eq. (17) for a given delay $\tau_2 > 0$. However, the introduction of an additional delay leads to a multiple-delay system complicating the analysis. Following [40], we apply the half-angle tangent substitution. Given an imaginary root $s = j\omega, \omega \in \mathbb{R}^+$, the two transcendental terms in Eq. (17) can be expressed as

$$e^{-j\tau_l\omega} = \cos(\theta_l) - j\sin(\theta_l), \theta_l = \tau_l\omega, l = 1, 2, \tag{24}$$

which can be rationalized by following substitutions

$$\cos(\theta_l) = \frac{1 - z_l^2}{1 + z_l^2}, \sin(\theta_l) = \frac{2z_l}{1 + z_l^2}, \tag{25}$$

with the mapping condition from z_l to τ_l as

$$z_l = \frac{\sin(\theta_l)}{1 + \cos(\theta_l)} = \tan\left(\frac{\theta_l}{2}\right) = \tan\left(\frac{\omega\tau_l}{2} + k\pi\right), k \in \mathbb{Z}. \tag{26}$$

From Eq. (26), one (z_1, z_2) pair yields infinitely many delay pairs (τ_1, τ_2) . Conversely, one delay pair (τ_1, τ_2) corresponds to one (z_1, z_2) pair only. Substituting Eqs. (24) and (25) into Eq. (17), the two transcendental terms of Eq. (17) retreat to two complex polynomial fractions in $z_l, l = 1, 2$. We then obtain a complex fractional polynomial equation in ω, g , and $z_l, l = 1, 2$, say $N_0(s = j\omega, g, z_1, z_2) = 0$, the numerator of which gives a new characteristic equation without transcendentality,

$$N(j\omega, g, z_1, z_2) = N_0(j\omega, g, z_1, z_2)(1 + z_1^2)(1 + z_2^2) = 0, \tag{27}$$

which is equivalent to Eq. (17) only at imaginary roots $s = \pm j\omega$, yielding the tuning mechanism of the MD-DDR in Theorem 2.

Theorem 2. For a given delay $\tau_2 > 0$, the tuned control parameter pair (g, τ_1) for the MD-DDR to completely suppress the vibrations at the frequency ω is governed by

$$\begin{cases} g^{[2]} = \frac{\mu v \zeta_a (z_2^2 + 1)(z_1^2 + 1)}{z_1^2 - z_2^2}, \\ \tau_{1,k}^{[2]} = \frac{2}{\omega} \left[\text{atan2} \left(\frac{2\zeta_a v \omega - z_2(\omega^2 - v^2)}{2\zeta_a v z_2 \omega - v^2 + \omega^2} \right) + (k - 1)\pi \right], \end{cases} \tag{28}$$

where $k = 1, 2, \dots, z_2 = \tan(\tau_2\omega/2)$, $\text{atan2}(\cdot) \in [-\pi, \pi]$, and z_1 is defined in Eq. (32) of the proof. **Proof.** The problem becomes seeking the parameter composition (ω, g, z_1) satisfying Eq. (27) for a given z_2 , and both real and imaginary parts of the left side of this equation should vanish yielding

$$N_R(\omega, g, z_1) = 2(z_1 - z_2)(1 - z_1 z_2)\omega g + \mu(z_1^2 + 1)(z_2^2 + 1)(\omega^2 - v^2) = 0, \tag{29}$$

$$N_I(\omega, g, z_1) = -2\omega [g(z_1^2 - z_2^2) - (z_2^2 + 1)(z_1^2 + 1)\zeta_a \mu v] = 0, \tag{30}$$

which are two linear polynomial equations in g . Discarding the cases where $g = 0$ and $\omega = 0$, solving Eq. (30) leads to the tuned gain $g^{[2]}$. Plugging $g = g^{[2]}$ into (29) results in a polynomial equation in z_1

$$\frac{[(z_1 + z_2)(v^2 - \omega^2) - 2v\zeta_a\omega(z_1 z_2 - 1)](z_1^2 + 1)(z_2^2 + 1)\mu}{z_1 + z_2} = 0. \tag{31}$$

Discarding the imaginary z_1 solution and the solution $z_1 = z_2$ that means $\tau_1 = \tau_2$ and thus null feedback force, we arrive at

$$z_1 = \frac{2\zeta_a v \omega - z_2(\omega^2 - v^2)}{2\zeta_a v z_2 \omega - v^2 + \omega^2}. \tag{32}$$

Deploying the four-quadrant inverse tangent $\text{atan2}(\cdot)$ to match the argument of the complex exponent $e^{-j\tau_l\omega}$ in (24), back substituting (32) into (26) yields the tuned delay $\tau_{1,k}^{[2]}$ of the MD-DDR. \square

Corollary 2. For a given coupled system and a branch number k , except for the jump points governed by the condition $\text{atan2}(\cdot) \in [-\pi, \pi]$, the tuned delay $\tau_{1,k}^{[2]}$ decreases as the frequency ω increases regardless of the τ_2 values.

Proof. Directly determining the analytical form of $\partial\tau_{1,k}^{[2]}/\partial\omega$ following Eq. (23) is cumbersome. Instead, we consider that

$$\frac{\partial\tau_{1,k}^{[2]}}{\partial\omega} = -\frac{\tau_{1,k}^{[2]}}{\omega} + \frac{2}{\omega[(z_1 + \pi(k - 1))^2 + 1]} \frac{\partial z_1}{\partial\omega}, \tag{33}$$

where we have

$$\frac{\partial z_1}{\partial\omega} = -\frac{\left((\omega^2 - v^2)^2 + 4v^2\omega^2\zeta_a^2 \right) \frac{\partial z_2}{\partial\omega} + 2v(z_2^2 + 1)(\omega^2 + v^2)\zeta_a}{(v^2 - \omega^2 - 2vz_2\omega\zeta_a)^2} \tag{34}$$

according to Eq. (32). Given that $\partial z_2/\partial\omega > 0$, one obtains $\partial z_1/\partial\omega < 0$ when $\omega > 0$ so that $\partial\tau_{1,k}^{[2]}/\partial\omega < 0$. \square

Remark 3. Different from that the tuned gain $g^{[1]}$ of the SD-DDR is always positive, the sign of the tuned gain $g^{[2]}$ of the MD-DDR is variable depending on the sign of $|z_1| - |z_2|$ as per Eq. (28). Thus, the polarity of the feedback actuation \bar{u}_{MD} could need to be reversed. Note that such polarity reversing can be achieved by swapping the values of the two delays $\bar{\tau}_1$ and $\bar{\tau}_2$ only when adopting the lumped velocity-based logic \bar{u}_V given the form of Eq. (16). As for the distributed control logic \bar{u}_{MD} , swapping the two delay values makes no sense due to the integral operation and the condition $\bar{\tau}_1 > \bar{\tau}_2$. \square

Remark 4. In addition to directly reversing the actuation polarity of \bar{u}_{MD} , an alternative approach from the software aspect can be the sign inverting control (SIC) [42], which additionally applies odd multiple of the half-cycle delay shifts so that the sign of the gain to be reversed can be reserved, i.e.,

$$-U_{MD}(s=j\omega) = -jg\omega(e^{-j\tau_1\omega} - e^{-j\tau_2\omega}) = jg\omega\left(e^{-j\omega\left(\tau_1 \pm \frac{(2k-1)\pi}{\omega}\right)} - e^{-j\omega\left(\tau_2 \pm \frac{(2k-1)\pi}{\omega}\right)}\right), k \in \mathbb{Z}. \tag{35}$$

Note that the SIC logic by shifting the delay values cannot apply to the SD-DDR since the symmetry of the two terms $e^{-j\tau_1\omega}$ and $e^{-j\tau_2\omega}$ no longer exists if $\tau_2 \equiv 0$, which also demonstrates that no negative tuned gain $g^{[1]} < 0$ is allowed agreeing with Remark 2. However, the SIC logic is not considered for simplicity since larger delays can lead to a longer transient process [4] and lower robustness [28]. In addition, the given analysis holds regardless of the gain polarity. \square

Remark 5. Notice that the two considered delay values $\bar{\tau}_1$ and $\bar{\tau}_2$ in practical uses have included the inevitable loop delay $\bar{\delta}$ caused by all operations of calculating, communicating, etc. That is, the actual output of $\bar{\tau}_1 > \bar{\delta}$ and $\bar{\tau}_2 > \bar{\delta}$ should be corrected as $\bar{\tau}_{i,COR} = \bar{\tau}_i - \bar{\delta}$, $i = 1, 2$ to achieve the expected vibration suppression performance. However, this correction is not explicitly considered in the given theoretical analysis for clarity, and we take it as a default operation of the controller. \square

Remark 6. In light of [36,37], another factor in practical numerical implementation that would affect the output of the tuned delay is the sampling time of the controller, which is $\Delta\bar{t} = 1/\bar{f}_{hz}$, where \bar{f}_{hz} is the sampling frequency. Note that $\Delta\bar{t} < \bar{\delta}$. The existence of $\Delta\bar{t}$ means that the actual output of a given delay $\bar{\tau}_i$, $i = 1, 2$ would be interpreted as

$$\bar{\tau}_{i,ACT} = \left\lceil \frac{\bar{\tau}_{i,COR}}{\Delta\bar{t}} \right\rceil \Delta\bar{t} + \bar{\delta}, \tag{36}$$

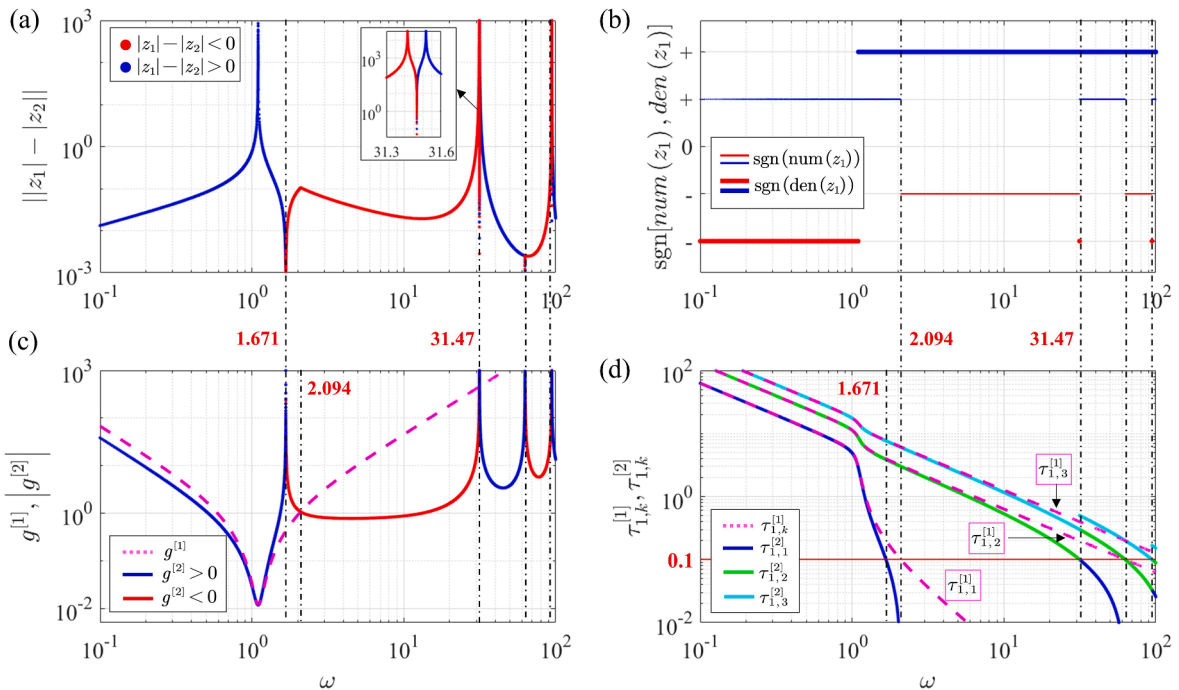


Fig. 2. (a). Variations of $|z_1| - |z_2|$ versus ω . (b). Sign variations of $\text{num}(z_1)$ and $\text{den}(z_1)$ versus ω . (c). Variations of $g^{[1]}$ and $g^{[2]}$ versus ω . (d). Tuned delays $\tau_{1,k}^{[1]}$ and $\tau_{1,k}^{[2]}$ with $k = 1, 2, 3$ versus ω , and red solid line denotes $\tau_1 = 0.1$.

where the notation $\lceil \cdot \rceil$ denotes the rounding function. Clearly, the effect of $\Delta\bar{\tau}$ can be significant when $\Delta\bar{\tau}$ is not negligible compared with $\bar{\tau}_i$ and when $\bar{\tau}_i$ is not an integer multiple of $\Delta\bar{\tau}$. Since $\bar{\tau}_2$ is a preselected value, the effect of $\Delta\bar{\tau}$ on implementing $\bar{\tau}_2$ can be limited by having $\bar{\tau}_{2,COR}/\Delta\bar{\tau} \in \mathbb{Z}^+ \cup 0$. However, the tuned delay $\bar{\tau}_{1,k}^{[2]}$ is a function of $\bar{\omega}$, so the rounding operation can cause errors, and such issues are more critical in the high-frequency band as per [Corollary 2](#). In this case, we can increase the branch number k to prolong the tuned delay $\bar{\tau}_{1,k}^{[2]}$ of the MD-DDR. However, for the SD-DDR, we will find that it always performs poorly in the high-frequency band regardless of the operability of the tuned parameters $(g^{[1]}, \tau_{1,k}^{[1]})$. Besides, a known alternative for [Eq. \(36\)](#) except for increasing k is to design an additional feedback filter as in [\[37\]](#). \square

4. Analysis of the tuned control parameters

In this part, we first analyze the tuned parameters and then demonstrate the issues of the SD-DDR and the benefits of the new MD-DDR. The example system is taken from the experimental setup in the SD-DDR studies of [\[36,37\]](#), with

$$\begin{aligned} \bar{m}_p &= 1.520\text{kg}, \bar{c}_p = 10.11\text{kg} \cdot \text{sec}^{-1}, \bar{k}_p = 1960\text{N} \cdot \text{m}^{-1}, \\ \bar{m}_a &= 0.223\text{kg}, \bar{c}_a = 1.273\text{kg} \cdot \text{sec}^{-1}, \bar{k}_a = 350\text{N} \cdot \text{m}^{-1}. \end{aligned} \quad (37)$$

The corresponding dimensionless parameters as per (4) are then $\mu = 0.1467$, $\zeta_p = 0.0926$, $\zeta_a = 0.072$, and $\nu = 1.103$.

4.1. Tuned parameter behavior

Selecting $\tau_2 = 0.1$ for instance, the two tuned parameter pairs $(g^{[1]}, \tau_{1,k}^{[1]})$, $(g^{[2]}, \tau_{1,k}^{[2]})$ and the associated intermediate variables (z_1, z_2) with respect to the frequency ω for the coupled system (37) are shown in [Fig. 2](#). Particularly, notations $\text{num}(z_1)$ and $\text{den}(z_1)$ in [Fig. 2\(b\)](#) means getting the numerator and the denominator of z_1 , respectively.

The two intermediate variables z_1 and z_2 when tuning the MD-DDR are compared in [Fig. 2\(a\)](#), and one sees that the frequency bands where $|z_1| > |z_2|$ and $|z_1| < |z_2|$ correspond to the cases $g^{[2]} > 0$ and $g^{[2]} < 0$ in [Fig. 2\(c\)](#), respectively. Also from [Fig. 2\(c\)](#), the tuned gain $g^{[1]}$ of the SD-DDR is always positive, and we have $g^{[1]} = -g^{[2]}$ at $\omega = 2.094$ so that the tuned delay of the MD-DDR satisfies $\tau_{1,1}^{[2]} \rightarrow 0$ and that of the SD-DDR satisfies $\tau_{1,1}^{[1]} = \tau_2$ at the identical frequency in [Fig. 2\(d\)](#), which is related to the symmetry of the two delay terms, see [Eq. \(16\)](#). We also point out that $g^{[2]} \rightarrow \infty$ as $\omega \rightarrow 1.671$, $\omega \rightarrow 31.47$, etc, due to the condition $\tau_{1,1}^{[2]} = \tau_2$ or equivalently $|z_1| = |z_2|$.

As for the tuned delays shown in [Fig. 2\(d\)](#), only the first three branches of $\tau_{1,k}^{[1]}$ and $\tau_{1,k}^{[2]}$ are compared without loss of generality. Both $\tau_{1,k}^{[1]}$ and $\tau_{1,k}^{[2]}$ decrease as ω increases regardless of the branch number k , thus verifying [Corollaries 1 and 2](#). Besides, $\tau_{1,k}^{[1]}$ is continuous while $\tau_{1,k}^{[2]}$ is piecewise continuous when varying ω for a given k . The continuity of $\tau_{1,k}^{[1]}$ results from the positive characteristics of $\tau_{1,1}^{[1]} > 0$ as mentioned in [Remark 1](#). As for the piecewise behavior of $\tau_{1,k}^{[2]}$, one can find that no positive values of $\tau_{1,1}^{[2]}$ exist within $\omega \in (2.094, 31.47)$ since $\text{num}(z_1) < 0$ holds in this frequency interval, see [Fig. 2\(b\)](#). Note that the function $\text{atan2}(\cdot)$ is periodic and the function value satisfies $\text{atan2}(\cdot) \in [-\pi, \pi]$, and thus the tuned delay $\tau_{1,2}^{[2]}$ resulting from the upward delay shift $2\pi/\omega$ by increasing k emerges within $\omega \in (2.094, 31.47)$. Furthermore, $\tau_{1,2}^{[2]}$ is continuous to $\tau_{1,1}^{[2]}$ at $\omega = 31.47$ since z_1 is continuous to ω at this frequency with a reversed sign as per [Eq. \(32\)](#) and see [Fig. 2\(b\)](#) also. Similar analyses apply to other segments of $\tau_{1,k}^{[2]}$.

4.2. Issues with the SD-DDR

Note that the delay $\tau_2 = 0.1$ corresponds to a dimensional value of $\bar{\tau}_2 = \tau_2/\bar{\omega}_p = 2.8\text{ms}$, and we take it as the smallest feedback loop delay $\bar{\delta}$ indicating that any practically meaningful $\bar{\tau}_1$ value of both the SD-DDR and the MD-DDR must satisfy $\bar{\tau}_1 \geq \bar{\tau}_2$ or equivalently $\tau_1 > \tau_2$. Furthermore, the tuned pairs $(g^{[2]}, \tau_{1,k}^{[2]})$ of the MD-DDR with $\tau_2 = 0.1$ can be interpreted as the corrected control parameters of the tuned SD-DDR to complement the loop delay $\bar{\delta}$.

Let us then consider the first branch $k = 1$ of $\tau_{1,k}^{[1]}$ of the tuned SD-DDR as this branch corresponds to the broadest operable frequency band and the strongest robustness, the so-called preferred branch [\[28\]](#). From [Fig. 2\(d\)](#), $\tau_{1,1}^{[1]}$ decreases as the frequency ω increases such that $\tau_{1,1}^{[1]} < \tau_2$ when $\omega > 2.094$. That is, any theoretical $\bar{\tau}_{1,1}^{[1]}$ value for $\omega > 2.094$ will be interpreted as $\bar{\delta}$ in a practical control loop, thus reducing the vibration suppression performance. However, the upper frequency bound $\omega = 2.094$ is still an optimistic value. As shown in [Fig. 2\(c\)](#), the agreement between the two tuned gains $g^{[1]}$ and $g^{[2]}$ reduces as ω increases, and the uncorrected gain $g^{[1]}$ is even of an inversed polarity to the practically required gain $g^{[2]}$ when $\omega > 1.671$. Consequently, one receives very poor vibration suppression performance when deploying SD-DDR within $\omega \in (1.671, 2.094)$, although the tuned delays $\tau_{1,1}^{[1]}$ in this frequency interval are achievable in practice. Given the differences between $g^{[1]}$ and $g^{[2]}$ when $\omega > 1.671$ from both aspects of polarity and gain values regardless of the branch number k , the operable frequency band for vibration suppression by the tuned SD-DDR is upper bounded by $\omega = 1.671$ at best, see also [Remark 6](#). Furthermore, the vibration suppression within $\omega < 1.671$ is incomplete due to the uncorrected

control parameter pair $(g^{[1]}, \tau_{1,k}^{[1]})$. Consequently, the limited operable frequency band and incomplete vibration suppression are the two main issues of the SD-DDR. Numerical studies for verification are prepared in Section 7.

Remark 7. We point out that the considered loop delay $\bar{\delta} = 2.8\text{ms}$ is of practical significance, considering that the sampling period of the controller in [36,37] has been explicitly signified as $\Delta\bar{t} = 1\text{ms}$. The increased values of $\bar{\delta}$ compared with $\Delta\bar{t}$ result from additional operations such as computations, data communication, etc., see also Remarks 5 and 6. \square

4.3. Benefits of the MD-DDR for parameter tuning

We next demonstrate the benefits of the MD-DDR for tuning control parameters. Considering that the tuned gain $g^{[2]}$ is achievable within a wide enough high-frequency band, e.g., $\omega \in (1.671, 31.47)$ in Fig. 2(c), the high-frequency vibration suppression performance of the MD-DDR is mainly governed by the tuned delay $\tau_{1,k}^{[2]}$. Let us then revisit Fig. 2(d), where the MD-DDR tuned with $k = 1$ is upper bounded by $\omega = 1.671$ due to the logic constraint $\tau_1 > \tau_2$, which can be solved by increasing k to prolong the tuned delay $\tau_{1,k}^{[2]}$ while suppressing the negative effects of the numerical implementation as per Remark 6. Consequently, hardware performance poses limited constraints to the operability of the MD-DDR.

Since the delay τ_2 can also be tunable online, the tuned pairs $(g^{[2]}, \tau_{1,k}^{[2]})$ of the MD-DDR corresponding to $\tau = 0.1$ and $\tau_2 = 0.2$ are compared in Fig. 3, and $\delta = \bar{\delta}/\bar{\omega}_p = 0.1$ is still taken as the inevitable loop delay so that the operable tuned delay $\tau_{1,k}^{[2]}$ of the MD-DDR must satisfy $\tau_{1,k}^{[2]} > \tau_2 > \delta$. From Fig. 3(c), increasing τ_2 narrows the maximum operable frequency band. Let us then focus on Fig. 3(a) and (b) for the tuned gain $g^{[2]}$, and one can find that the selecting $\tau_2 = 0.2$ shifts the frequencies where $g^{[2]} \rightarrow \infty$ to $\omega \rightarrow 1.411, \omega \rightarrow 15.76$, etc. That is, we can real-time tune τ_2 according to the actual excitation frequency to avoid the infinite tuned gain values $g^{[2]} \rightarrow \infty$, which benefits feedback actuation and thus vibration suppression. From this perspective, tuning τ_2 , in fact, extends the operable frequency band since the MD-DDR is mainly designed to suppress the single-frequency vibration, and the vibration at any frequency corresponding to an achievable tuned delay $\tau_{1,k}^{[2]}$ can now be completely suppressed if the coupled system is stable. For instance, we can select $\tau_2 = 0.1$ and $\tau_2 = 0.2$ to handle the vibrations at $\omega = 1.411$ and $\omega = 1.671$, respectively. Fig. 3 provides guidelines for selecting τ_2 according to actual excitation frequencies. Note also from Eq. (15) that excitation amplitudes do not affect feedback actuation tuning since the excitation does null work when the complete vibration suppression $x_p = 0$ is achieved.

5. Stability analysis

We have shown that any operable tuned control parameter composition must fit the performance of the practical controller or actuator. Let us next consider the operability concerning the stability issues given that the feedback actuation makes sense only if the coupled system is stable, i.e., all the characteristic roots of Eq. (19) have negative real parts.

5.1. Stability boundary

Even the injection of a single time delay into the system leads to infinitely many characteristic roots, and thus evaluating stability by exhaustively determining the spectrum is impractical, let alone the multiple-delay case associated with the considered MD-DDR. To

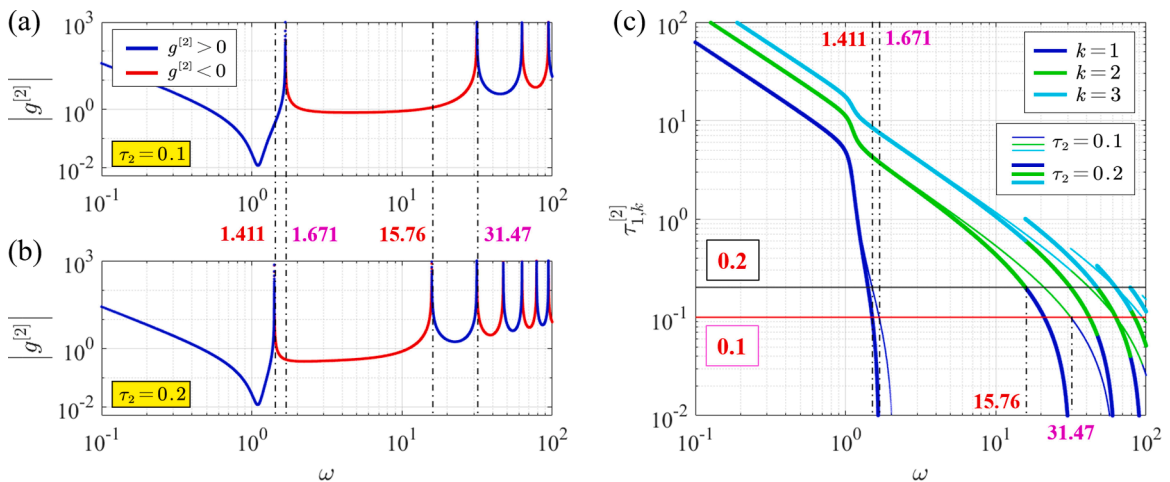


Fig. 3. (a). The variations of $|g^{[2]}|$ versus ω . (b). The delay $\tau_{1,k}^{[2]}$ with $k = 1, 2, 3$ versus ω , where the black and red solid line denotes $\tau_1 = 0.2$ and $\tau_1 = 0.1$. Thick and thin curves correspond to the cases $\tau_2 = 0.2$ and $\tau_2 = 0.1$, respectively.

this end, we follow the D-subdivision method [43], the core of which is that the stability loss and regain must occur at the critical moment when the characteristic Eq. (19) exhibits at least a pair of imaginary roots. Hence, the parameter pairs (g, τ_1) for a given τ_2 corresponding to such critical moments are defined as stability boundaries, leading to Theorem 3.

Theorem 3. Given a delay τ_2 , the stability boundaries of the coupled system Eq. (19) on the $g \times \tau_1$ plane can be exhaustively determined by sweeping $\omega_{CS} \in \mathbb{R}^+$ as

$$\begin{cases} g^{[CS]} = \frac{\mu(z_1^2 + 1)(z_2^2 + 1)((v^2 - \omega_{CS}^2)\zeta_p + \zeta_a(1 - \omega^2) - \mu\omega_{CS}^2\zeta_a)}{(z_1 - z_2)((1 - \omega_{CS}^2)(z_1 + z_2) + 2\zeta_p\omega_{CS}(z_1z_2 - 1))}, \\ \tau_{1,r}^{[CS]} = \frac{2}{\omega} \left[\text{atan2}\left(\frac{-\gamma_0}{\gamma_1}\right) + (r - 1)\pi \right], r \in Z, \end{cases} \quad (38)$$

where $z_2 = \tan(\tau_2\omega/2)$, and $z_1 = -\gamma_0/\gamma_1$, see proof for the definitions of γ_0 and γ_1 , two polynomials in ω_{CS} . **Proof.** First, $s = 0$ is obviously not a root of the characteristic Eq. (19). Similar to Theorem 2, we then plug the half-angle tangent substitution Eq. (25) into Eq. (19) for its equivalent polynomial form at the imaginary roots $s = \pm j\omega_{CS}$, $\omega_{CS} \in \mathbb{R}^+$, and both real and imaginary parts of the numerator of the resulting complex polynomial should vanish yielding

$$CE_R(\omega_{CS}, g, z_1, z_2) = \sum_{i=0}^1 a_i(\omega_{CS}, z_1, z_2)g^i = 0, \quad (39)$$

$$CE_I(\omega_{CS}, g, z_1, z_2) = \sum_{i=0}^1 \beta_i(\omega_{CS}, z_1, z_2)g^i = 0, \quad (40)$$

two linear equations in g , where a_i and β_i are polynomial coefficients. Solving Eq. (40) leads to $g^{[CS]}$, which can be further plugged into Eq. (39) to give a polynomial equation in (ω_{CS}, z_1, z_2) ,

$$Q_0(\omega_{CS}, z_1, z_2) = \mu(z_1^2 + 1)(z_2^2 + 1)Q(\omega_{CS}, z_1, z_2) = 0. \quad (41)$$

Since $(z_1, z_2) \in \mathbb{R}^2$, the last factor needs to vanish, leading to

$$Q(\omega_{cs}, z_1, z_2) = \gamma_1(\omega_{cs}, z_2)z_1 + \gamma_0(\omega_{cs}, z_2) = 0, \quad (42)$$

where γ_1 and γ_0 are self-evident polynomial coefficients. The unique solution of Eq. (41) is then

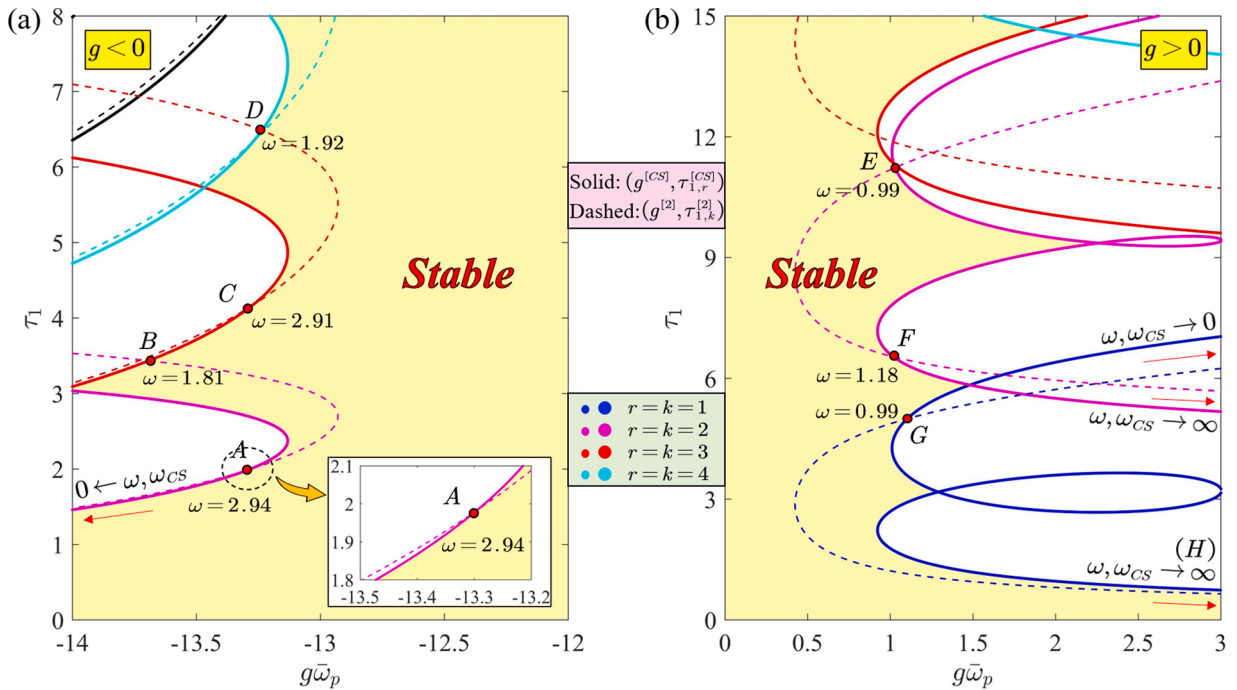


Fig. 4. Stability maps of the coupled system (37) with $\tau = 0.2$. Thick and thin curves denote stability boundaries $(g^{[CS]}, \tau_{1,r}^{[CS]})$ and the tuned parameter pairs $(g^{[2]}, \tau_{1,k}^{[2]})$ of the MD-DDR, respectively. Colored regions are stable. (a). $g < 0$. (b). $g > 0$.

$$z_1(\omega_{CS}, z_2) = \frac{\gamma_0}{\gamma_1} = \frac{\sum_{i=0}^6 \eta_{0,i}(\omega_{CS}, z_2) \omega_{CS}^i}{\sum_{i=0}^6 \eta_{1,i}(\omega_{CS}, z_2) \omega_{CS}^i}, \tag{43}$$

where $\eta_{1,i}$ and $\eta_{0,i}$ are polynomials in (ω_{CS}, z_2) , and therefore z_1 is a function in a single variable ω_{CS} for a given τ_2 . Back substituting z_1 into Eqs. (38) and (25) obtains the stability boundaries in ω_{CS} . \square

Definition 1. (Root tendency (RT) [44]). Stability boundaries specify the parameter compositions (g, τ_1, τ_2) where imaginary roots appear, i.e., $s = \pm j\omega_{CS}$, while the shifting direction of the imaginary roots as time-domain parameters cross the stability boundaries is still unclear. The root tendency is defined as

$$RT(\omega, \lambda) = \text{sgn} \left(\Re \left(\frac{\partial s}{\partial \lambda} \right)_{s=j\omega_{CS}} \right), \frac{\partial s}{\partial \lambda} = - \frac{\frac{\partial CE(s, \lambda)}{\partial \lambda}}{\frac{\partial CE(s, \lambda)}{\partial s}}, \tag{44}$$

where ω_{CS} is used to discriminate it from the vibration frequency ω , $\lambda \in [g, \tau_1, \tau_2]$ denotes the crossing variable. Clearly, $RT = +1$ and $RT = -1$ corresponds to a destabilizing and stabilizing crossing, respectively. \square

5.2. Stability map

For the coupled system Eq. (37), selecting $\tau_2 = 0.2$ leads to the stability boundaries $(g^{[CS]}, \tau_{1,r}^{[CS]})$ shown as the thick solid curves in Fig. 4, where the abscissa denoting the gain g is scaled up by the factor $\bar{\omega}_p$ to facilitate demonstration.

Fig. 4(a) and (b) depict the cases where $g < 0$ and $g > 0$, respectively. Clearly, the coupled system is always stable when $g = 0$ since no feedback actuation is applied in this case, and stability reserves as $g \rightarrow 0^+$ given that the infinitesimal actuation force is unable to alter coupled system dynamics. Note that stability only switches at stability boundaries $(g^{[CS]}, \tau_{1,r}^{[CS]})$ where at least one pair of imaginary roots appears, and thus the shown colored regions containing the line $g \rightarrow 0^+$ must be stable. As we cross the stability boundaries, the shifting direction of the associated imaginary roots can be determined by the RT defined in Eq. (44), and the crossings with $RT = +1$ and $RT = -1$ increase and decrease the number of unstable characteristic roots, respectively. By counting the number of such crossings, stable regions can be exhaustively determined. Obviously, any operable control parameter (g, τ_1) of the MD-DDR for a given τ_2 must lie within the stable regions.

5.3. Operable frequency interval for complete vibration suppression

The tuned control parameter pairs $(g^{[2]}, \tau_{1,k}^{[2]})$ of the MD-DDR constitute the thin dashed curves in Fig. 4, and meaningful ones must lie within the stable regions. The stable segments of the $(g^{[2]}, \tau_{1,k}^{[2]})$ curves provide another design criterion in addition to the control logic constraint $\tau_{1,k}^{[2]} > \tau_2$ for the tuned MD-DDR to yield the desired complete vibration suppression.

Taking into account both stability issues and logic constraints, four operable segments are marked in Fig. 4 for demonstration, i.e., *AB*, *CD*, *EF*, and *GH*. Note that the upper bound *H* is not shown due to coordinate limitation, and it corresponds to the intersection of the tuned curve $(g^{[2]}, \tau_{1,1}^{[2]})$ and the stability boundary $(g^{[CS]}, \tau_{1,1}^{[CS]})$ or the intersection of $\tau_{1,1}^{[2]}$ and τ_2 , whichever exhibits a smaller tuned delay $\tau_{1,1}^{[2]}$. From Fig. 2 and Fig. 3, continuous curves of tuned pairs $(g^{[2]}, \tau_{1,k}^{[2]})$ correspond to continuous variations of the vibration frequency ω regardless of k . Thus, the operable frequency interval for each operable $(g^{[2]}, \tau_{1,k}^{[2]})$ segment is governed by the two frequencies corresponding to the two segment ends.

For the intersection of the curves $(g^{[2]}, \tau_{1,k}^{[2]})$ and $(g^{[CS]}, \tau_{1,k}^{[CS]})$, each intersection corresponds to an identical pair (g, τ_1) while two different pairs of imaginary roots for the MD-DDR and the coupled system, leading to

$$\begin{cases} g^{[2]}(\omega, \tau_2) - g^{[CS]}(\omega_{CS}, \tau_2) = 0, \\ \tau_{1,k}^{[2]}(\omega, \tau_2, k) - \tau_{1,r}^{[CS]}(\omega_{CS}, \tau_2, r) = 0, \end{cases} \tag{45}$$

where $(\omega, \omega_{CS}) \in \mathbb{R}^{2+}$ and $\omega \neq \omega_{CS}$. Eq. (45) can be numerically solved once given (r, k, τ_2) . As for the frequency associated with the

Table 1

Frequency intervals corresponding to the four selected $(g^{[2]}, \tau_{1,k}^{[2]})$ segments in Fig. 4.

Segment	<i>AB</i>	<i>CD</i>	<i>EF</i>	<i>GH</i>
Tuned gains at two ends	[- 0.3812, - 0.3703]	[- 0.3697, - 0.3686]	[0.0284, 0.0286]	[0.0306, ∞]
Tuned delay interval	[1.9820, 3.4656]	[4.1614, 6.4843]	[6.5363, 11.2342]	[0.2, 4.9910]
Stable frequency interval	[1.8064, 2.9372]	[1.9169, 2.9147]	[0.9937, 1.1786]	[0.9875, 1.4110]

intersection of $\tau_{1,1}^{[2]} = \tau_2$, it can be obtained by combining the condition $z_1 = z_2$ with Eq. (32), yielding

$$(\omega^2 - v^2)\tan(\tau_2\omega) - 2\zeta_a v\omega = 0. \tag{46}$$

The results of the four mentioned segments are given in Table 1. We can find that operable frequency intervals corresponding to segments *CD* and *EF* are covered by those to segments *AB* and *GH*, respectively, indicating that a smaller tuned delay yields a broader operable frequency band. The same conclusion is also observed for the lumped-type DRs [28]. Therefore, the two segments *AB* and *GH* yielding the smallest positive tuned delay $\tau_{1,k}^{[2]}$ are preferable for the MD-DDR design. Note that the tuned gain $g^{[2]}$ on segments *AB*, *CD*, and *EF* varies within a relatively narrow range. The resulting variations of the operable frequency intervals imply that time delay can significantly affect system dynamics. Next, the operable frequency intervals for the two preferable segments *AB* and *GH* with sweeping $\tau_2 \in [0.1, 1]$ are shown in Fig. 5.

Fig. 5 shows that both the upper and the lower bounds of the operable frequency intervals decrease as τ_2 increases. Since τ_2 is a real-time tunable parameter and since the MD-DDR is designed to handle the single-frequency vibration, the decreased lower bounds indicate that tuning τ_2 extends the operable frequency band. Moreover, note that an unstable frequency gap exists between *H* and *A*, which deserves much attention when handling vibrations at a variable frequency, and obviously, this gap can be filled by tuning τ_2 . Furthermore, recall from Section 4.2 that the conventional SD-DDR yields vibration suppression (even incomplete) within $\omega < 1.671$ for $\delta = 0.1$, and the lower operable frequency bound of the SD-DDR due to stability issues can be found similarly to Eq. (45) as $\omega = 1.0063$, see Fig. 5. The extended operable frequency band of the MD-DDR in comparison verifies the benefits of actively tuning the loop delay. We also stress that the obtained theoretical operable frequency interval in practical uses must additionally consider system uncertainties, actuator dynamics, etc. Since the values of τ_2 can be manipulated online, how to select it to expedite the transient process is considered next.

6. Optimal τ_2 selection for expedited transient process

The idea of treating the transient response speed as an optimization index has been considered in [11,29,31] for the DR with different control logic or mechanical construction. The key is to determine the control parameter composition (g, τ_1, τ_2) that places the dominant (i.e., the rightmost) characteristic roots of the coupled system Eq. (19), say s_{dom} , furthest into the left half of the complex plane, as the settling time of a linear system can be approximated by

$$\bar{t}_s = -\frac{4}{\Re(\bar{s}_{dom})} = -\frac{4}{\Re(s_{dom}\bar{\omega}_p)} [\text{sec}], \Re(\bar{s}_{dom}) < 0, \tag{47}$$

where $\bar{s}_{dom} = s_{dom}\bar{\omega}_p$ and $\Re(\cdot)$ means getting the real part similar to Eq. (44). Since the closed-form spectrum of (19) does not exist, previous studies apply brute-force sweeping procedures with sufficiently dense grids to determine the optimal parametric composition for the smallest $\Re(s_{dom})$. Alternatively, such calculations can be simplified by also taking the imaginary part of s_{dom} into account.

6.1. Conventional procedure for tuning τ_2 for expedited transient process

For the coupled system Eq. (37) with $\bar{\omega}_p = 35.91\text{rad/sec}$, the vibration frequency $\bar{\omega} = 6.5\text{Hz}$ (i.e., $\omega = \bar{\omega}/\bar{\omega}_p = 1.137$) is considered as an example. The tuned pairs $(g^{[2]}, \tau_{1,k}^{[2]})$ and the real and imaginary parts of the dominant characteristic root s_{dom} with sweeping τ_2 are shown in Fig. 6.

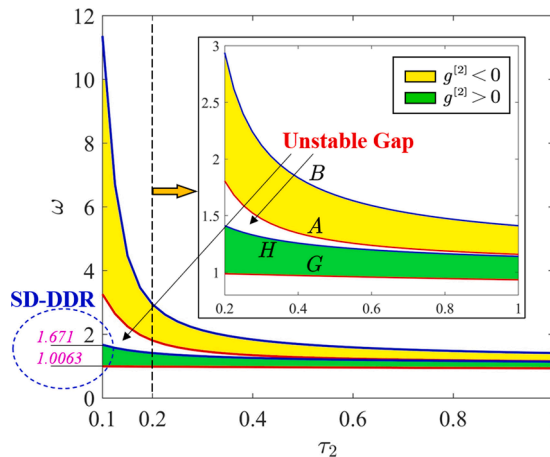


Fig. 5. Operable frequency intervals associated with the smallest tuned delay $\tau_{1,k}^{[2]}$ for $g > 0$ (green) and $g < 0$ (yellow).

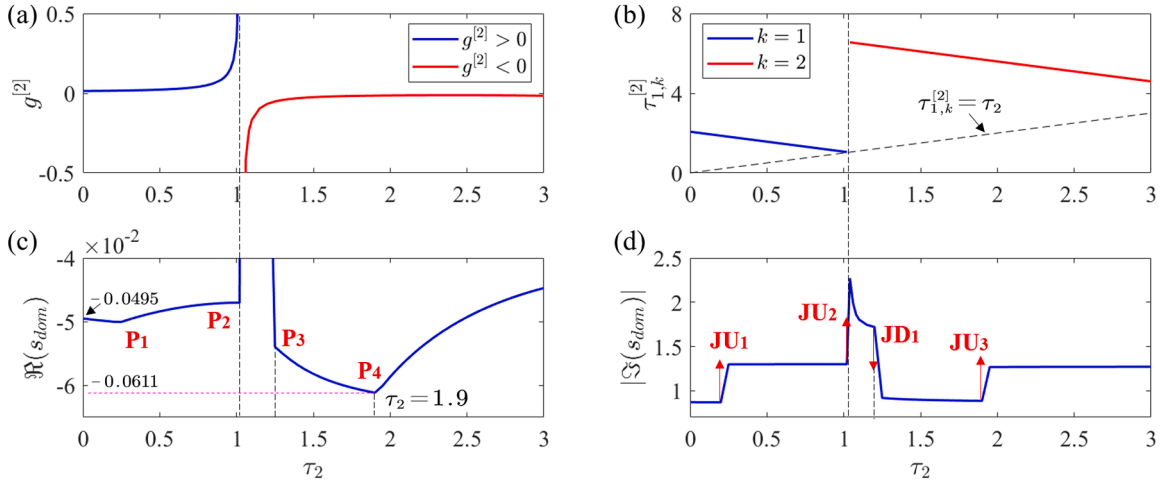


Fig. 6. (a). Tuned gain $g^{[2]}$ versus τ_2 . (b). Tuned delay $\tau_{1,k}^{[2]}$ versus τ_2 . (c). The real part of the dominant s_{dom} versus τ_2 . (d). The imaginary part of the dominant s_{dom} versus τ_2 .

Only the smallest tuned delays satisfying $\tau_{1,k}^{[2]} > \tau_2$ are considered in Fig. 6. Note that the tuned delay $\tau_{1,1}^{[2]}$ jumps up around $\tau_2 = 1.05$, and we have $|g^{[2]}| \rightarrow \infty$ at this τ_2 value agreeing with Eq. (28). Besides, results in Fig. 6(c) and (d) are obtained following [11,29,31] by sweeping the QPmR (Quasi-Polynomial mapping based Rootfinder) algorithm [45], which approximates the spectrum of a quasi-polynomial equation within a given complex region at a designated accuracy.

From Fig. 6(c), increasing τ_2 first shifts the dominant root s_{dom} leftward and then rightward. Subsequently, s_{dom} jumps to the right half of the complex plane when $\tau_2 \in [1.05, 1.25]$ leading to instability. As τ_2 further increases, stability recovers implying that delay does not always act as a negative factor causing destabilization. Let us then focus on the point $\tau_2 = 1.9$, where $\Re(s_{dom})$ reaches a minimum $\Re(s_{dom}) = -0.0611$ or $\Re(\bar{s}_{dom}) = -2.1941$, thus yielding the approximate settling time $\bar{t}_s = 1.8231\text{sec}$ as per Eq. (47). Thus, \bar{t}_s is reduced by 19% compared to the case $\tau_2 = 0$ where $\Re(s_{dom}) = -0.0495$ so that $\bar{t}_s = 2.2503\text{sec}$. Clearly, the accuracy of the optimal delay $\tau_2 = 1.9$ directly depends on the density of sweeping grids, so conservative results can be obtained at best, even at a high computational cost for sweeping. Combining with the previously overlooked variations of the imaginary part of s_{dom} shown in Fig. 6(d), such a brute-force optimization can be simplified.

6.2. Dominant root locus

From Fig. 6(d), the positive imaginary part of s_{dom} labeled as $|\Im(s_{dom})|$ jumps up three times and jumps down once as τ_2 varies. We then revisit Fig. 6(c), where $\Re(s_{dom})$ is not smoothly continuous at four τ_2 values that are related to the jump phenomena of $|\Im(s_{dom})|$. In

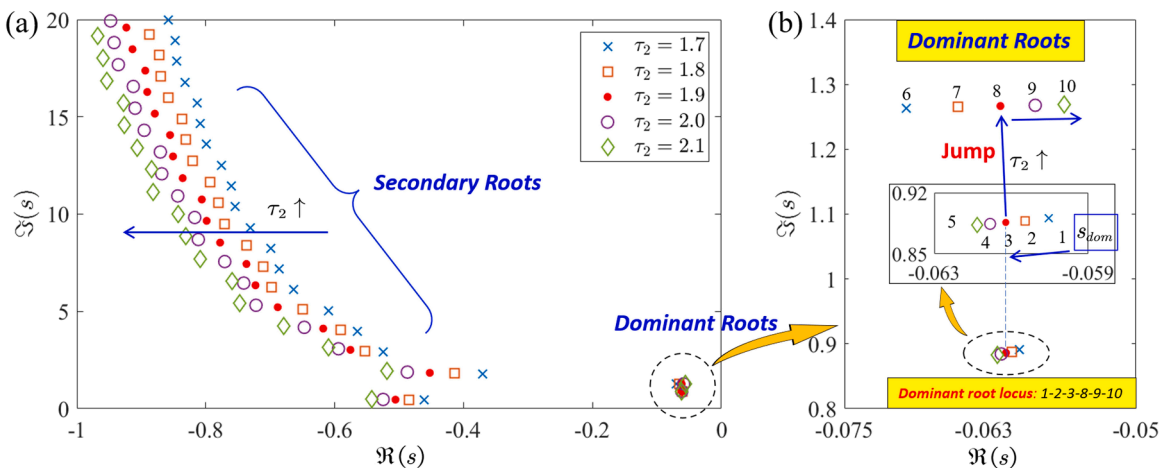


Fig. 7. (a). Spectra of the coupled system Eq. (19) concerning five control parameter compositions $(\tau_2, g^{[2]}, \tau_{1,2}^{[2]})$ for $\omega = 1.137$ and $\tau_2 = [1.7, 1.8, 1.9, 2.0, 2.1]$. (b). The zoomed plot of (a).

particular, the non-smooth point P_2 and the associated jump JU_2 are caused by the condition $\tau_{1,k}^{[2]} > \tau_2$ as in Fig. 6(b). Since characteristic roots move smoothly as system parameters smoothly vary according to the root continuity rule [43], we consider the non-smooth mechanism of P_1, P_2 , and P_4 (or equivalently JU_1, JD_1 , and JU_3). Taking P_4 that corresponds to the optimal delay $\tau_2 = 1.9$ obtained by numerical sweeping as an example, the spectra of Eq. (19) concerning five τ_2 values or more precisely five $(\tau_2, g^{[2]}, \tau_{1,2}^{[2]})$ compositions around $\tau_2 = 1.9$ is shown in Fig. 7.

Only the upper half of the complex plane is shown in Fig. 7 due to symmetry. Since system performance is dictated by the rightmost characteristic roots, let us focus on the set of dominant roots zoomed in Fig. 7(b). Note that two root loci exist in Fig. 7(b), i.e., 1-2-3-4-5 and 6-7-8-9-10, each of which is continuous as τ_2 varies as expected. However, this is not the case for the dominant root s_{dom} , the locus of which follows 1-2-3-8-9-10, i.e., s_{dom} jumps from the lower root locus to the higher one. Hence, continuous variations of $(\tau_2, g^{[2]}, \tau_{1,2}^{[2]})$ lead to a discontinuous locus of s_{dom} agreeing with Fig. 6(c) and (d). Since the two root loci 1-2-3-4-5 and 6-7-8-9-10 are continuous and in opposite directions, if the dominant root s_{dom} jumps from one locus to the other, the critical moment when the jump occurs must correspond to two positions that share an identical real part on two root loci. Besides, such an identical real part yields the minimum $\Re(s_{dom})$ labeled as $\min(\Re(s_{dom}))$. More specifically, the coupled system (19) exhibits a leftmost s_{dom} when its first two pairs of the rightmost characteristic roots have an identical real part but two distinctive imaginary parts and when the associated root loci evolve in opposite directions.

6.3. Exact optimizing procedure based on dominant root locus

Based on the observation of the dominant root locus, we substitute $s = \sigma + j\varpi, \sigma \in \mathbb{R}, \varpi \in \mathbb{R}^+$ into the characteristic equation (9), and both the real and imaginary parts of the resulting complex equation should vanish yielding

$$\begin{cases} CE_R^i(\sigma, \varpi, g, \tau_1, \tau_2) = \Re(CE(s = \sigma + j\varpi)) = 0, \\ CE_I^i(\sigma, \varpi, g, \tau_1, \tau_2) = \Im(CE(s = \sigma + j\varpi)) = 0, \end{cases} \quad (48)$$

where the superscript $(\cdot)^i$ is used to discriminate Eq. (48) from Eqs. (39) and (40). We focus on the upper half of the complex plane and denote the mentioned two pairs of characteristic roots whose real parts share $\min(\Re(s_{dom}))$ as

$$\begin{cases} s_1 = \sigma_{opt} + j\varpi_1, \\ s_2 = \sigma_{opt} + j\varpi_2, \end{cases} \quad (49)$$

where $\sigma_{opt} = \min(\Re(s_{dom}))$, and $(\varpi_1, \varpi_2) \in \mathbb{R}^{2+}, \varpi_1 \neq \varpi_2$. Plugging s_1 and s_2 into Eq. (48) leads to

$$\begin{cases} CE_R^i(\sigma_{opt}, \varpi_1, g, \tau_1, \tau_2) = 0, \\ CE_R^i(\sigma_{opt}, \varpi_2, g, \tau_1, \tau_2) = 0, \\ CE_I^i(\sigma_{opt}, \varpi_1, g, \tau_1, \tau_2) = 0, \\ CE_I^i(\sigma_{opt}, \varpi_2, g, \tau_1, \tau_2) = 0. \end{cases} \quad (50)$$

Given a vibration frequency ω , the pair (g, τ_1) is tuned according to Theorem 2 and thus is parameterized in τ_2 . That is, four

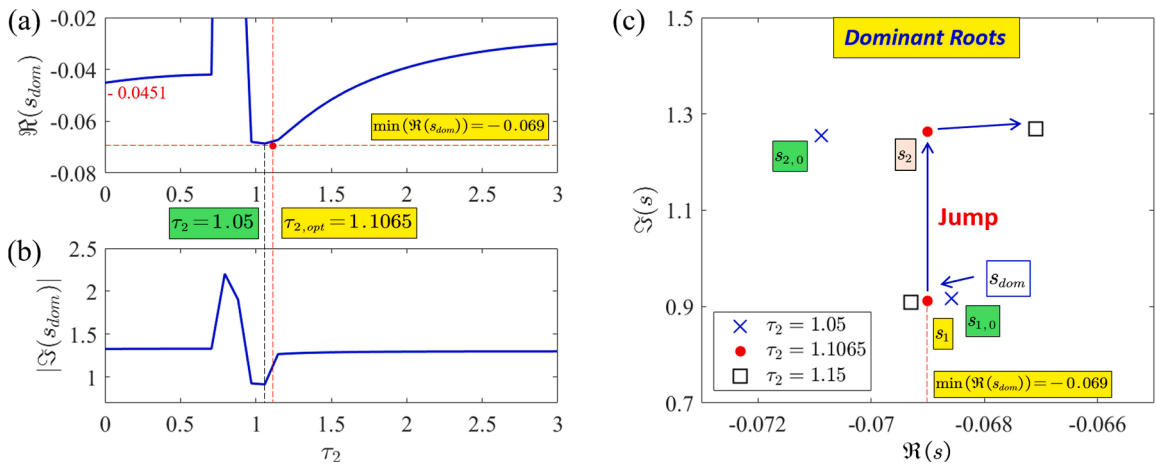


Fig. 8. Spectral analysis of the coupled system Eq. (19) when the MD-DDR is tuned for $\omega = 1.17$ and $\tau_2 \in [0, 3]$. (a). $\Re(s_{dom})$ versus τ_2 . (b). $\Im(s_{dom})$ versus τ_2 . (c). Dominant root locus sampled at three τ_2 values.

unknowns $(\sigma_{opt}, \varpi_1, \varpi_2, \tau_2)$ are governed by four equations in Eq. (50), and therefore can be numerically solved. In addition, the results obtained by the QPmR algorithm provide a good initial guess to benefit convergence. As a result, the exact optimal τ_2 for the leftmost s_{dom} can be corrected as $\tau_{2,opt} = 1.9131$ leading to $\min(\Re(s_{dom})) = -0.0612$ and $\bar{t}_s = 1.8201$ sec.

Remark 8. Note that Eq. (50) only considers a special case to determine the leftmost s_{dom} or the associated optimal delay τ_2 since the condition that the leftmost s_{dom} occurs at the critical moment when s_{dom} jumps from one root locus to another is not guaranteed. The benefit is that the sweeping grids of the QPmR algorithm now do not have to be sufficiently dense at first. Once we have obtained the information that the minimum $\min(\Re(s_{dom}))$ could correspond to a jump phenomenon by analyzing variations of $|\Im(s_{dom})|$ as in Fig. 6 (c) and (d), Eq. (50) determines the exact or non-conservative solution at a very small computational cost. However, the problem of exact determination of the leftmost s_{dom} without such features remains open. □

6.4. Case study

Let us consider another frequency $\omega = 1.17$ to clarify the calculation procedure using Eq. (50). We are now allowed to sweep using the QPmR algorithm in sparse grids, yielding the s_{dom} locus shown in Fig. 8(a) and (b). From Fig. 8(a), sparse numerical sweeping gives an optimal delay $\tau_2 = 1.05$. Since $\Re(s_{dom})$ is not smoothly continuous at this τ_2 value and since $|\Im(s_{dom})|$ jumps simultaneously as per Fig. 8(b), we can conclude that the jump phenomenon must occur on the dominant root locus. We then check the spectrum at $\tau_2 = 1.05$ leading to two markers labeled as $s_{1,0}$ and $s_{2,0}$ in Fig. 8(c). Using $s_{1,0}$ and $s_{2,0}$ together with $\tau_2 = 1.05$ as the initial guess, Eq. (50) can be numerically solved yielding $\tau_{2,opt} = 1.1065$. The corresponding dominant roots are labeled as s_1 and s_2 , real parts of which are identical as expected. Moreover, slightly increasing τ_2 from $\tau_{2,opt}$ undesirably shifts s_{dom} rightward, and thus $\tau_{2,opt} = 1.1065$ can be claimed to be optimal for the fastest transient process. Compared to the reduced case $\tau_2 = 0$ where $\Re(s_{dom}) = -0.0451$, we have $\Re(s_{dom}) = -0.069$ at $\tau_2 = \tau_{2,opt}$ so that the settling time is reduced by 34.64%, again demonstrating the strength of the MD-DDR by manipulating the loop delay.

At last, the optimization procedure in Fig. 8 is performed on a standard laptop with an Intel i7-6700HQ CPU and 16 GB RAM, and the overall time cost for $\tau_{2,opt}$ is less than 1.3 sec with MATLAB 2020b. It is easy to imagine the required higher computational costs if we search the optimum $\tau_{2,opt} = 1.1065$ at the fourth decimal precision via brute-force sweeping (Note that the precision of $\tau_{2,opt}$ by numerical solving is infinite, and it is truncated with four decimal places due to space limitation).

Remark 9. In fact, the feature that the leftmost dominant root s_{dom} could correspond to a jump phenomenon on its locus has been shown before, but it has not yet been utilized for optimization. One can find from Fig. 18 of [29], Fig. 6 of [31], and most figures of [11] that the leftmost s_{dom} of the associated coupled systems either corresponds to two pairs of characteristic roots sharing an identical real part or the variations of $\Re(s_{dom})$ is non-smooth at the optimized parameters. Hence, this section provides an exact optimizing procedure in those cases while keeping the computational cost at a low level. □

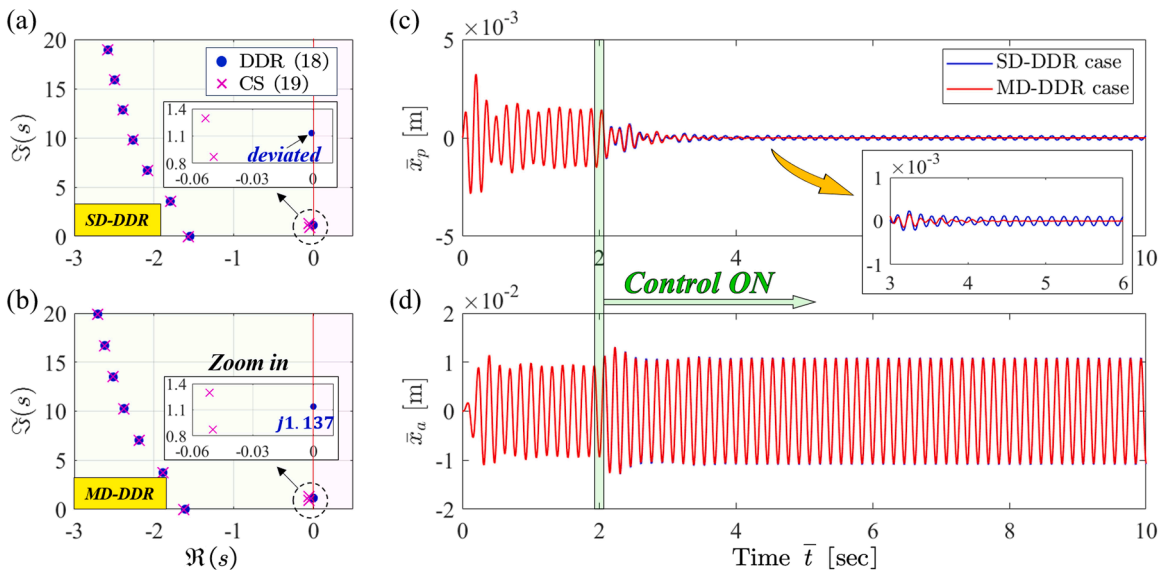


Fig. 9. (a) and (b) represent the spectra in the SD-DDR and MD-DDR cases, respectively, where the legend ‘CS’ represents the coupled system. The dynamics of the coupled system when deploying the SD-DDR and MD-DDR are compared in (c) and (d), where the feedback actuation is activated at $\bar{t} = 2$ sec.

7. Simulation

Simulations are performed to further demonstrate the benefits of the newly introduced delay $\bar{\tau}_2$ or equivalently τ_2 . In what follows, the coupled system considered is governed by (37), the smallest inevitable loop delay is taken as $\bar{\delta} = 2.8\text{ms}$ (i.e., $\delta = \bar{\delta}\bar{\omega}_p = 0.1$) as per Remark 7, and the excitation force \bar{f} applied on the primary structure is in the harmonic form of $\bar{f} = \bar{A}\sin(\bar{\omega}\bar{t})$ with a constant amplitude $\bar{A} = 4\text{N}$ following [36,37]. Simulations are based on MATLAB Simulink. See Appendix A for the construction of the multiple-distributed-delay operation, and all Simulink models are given in Appendix B.

7.1. Corrected tuned parameters for complete vibration suppression

Deploying the SD-DDR to suppress the vibration at the frequency $\bar{\omega} = 6.5\text{Hz}$ (i.e., $\omega = \bar{\omega}/\bar{\omega}_p = 1.137$), the preferred first branch of the control parameter pair is tuned by Theorem 1 to be $(g^{[1]}, \tau_{1,1}^{[1]}) = (0.0137, 2.062)$, leading to the dimensional form of $(\bar{g}^{[1]}, \bar{\tau}_{1,1}^{[1]}) = (g^{[1]}\bar{\omega}_p\bar{m}_p, \tau_{1,1}^{[1]}/\bar{\omega}_p) = (0.748\text{kg} \cdot \text{s}^{-1}, 57.5\text{ms})$. Dynamics of the coupled system are shown as blue curves in Fig. 9(c) and (d), and the associated numerical spectra by the QPmR algorithm [45] are given in Fig. 9(a) and (b).

The blue curve in Fig. 9(c) shows that the primary structure is settled by the SD-DDR activated at $\bar{t} = 2\text{sec}$. We can also find that some small residual vibrations exist, so the suppression is incomplete, which results from the fact that resonator states within the time interval $[\bar{t} - \bar{\delta}, \bar{t}]$ are always blinded to the SD-DDR due to causality. The incomplete vibration suppression is also reflected in the spectrum of the SD-DDR shown as the blue markers in Fig. 9(a), where the rightmost roots of the SD-DDR deviate from the imaginary axis, making the magnitude of the transfer function G defined in Eq. (7) non-zero. To this end, the proposed control logic u_{MD} in Eq. (12) takes the loop delay $\bar{\delta}$ into account. Selecting $\tau_2 = \delta = 0.1$, the tuned SD-DDR is corrected by Theorem 2, leading to the MD-DDR tuned with $(\bar{g}^{[2]}, \bar{\tau}_{1,1}^{[2]}) = (0.7905\text{kg} \cdot \text{s}^{-1}, 54.8\text{ms})$. The corresponding system dynamics are superposed as the red curves in Fig. 9(c) and (d), where the ideal vibration suppression is achieved. Besides, a pair of imaginary roots of the MD-DDR appears exactly agreeing with the vibration frequency $\omega = 1.137$, see Fig. 9(b). The rightmost characteristic roots of the coupled system (19) having negative real parts verify the stability map shown in Fig. 5.

7.2. Extended operable high-frequency band by tuning τ_2

We now increase the frequency to $\bar{\omega} = 13\text{Hz}$ (i.e., $\omega = 2.27$) to test the vibration suppression performance in the high-frequency band. The parameter pair of the tuned SD-DDR for $k = 1$ is then found to be $(\bar{g}^{[1]}, \bar{\tau}_{1,1}^{[1]}) = (76.35\text{kg} \cdot \text{s}^{-1}, 2.2\text{ms})$. Since $\bar{\tau}_{1,1}^{[1]} = 2.2\text{ms} < \bar{\delta}$, the delay parameter $\bar{\tau}_{1,1}^{[1]}$ would be interpreted as $\bar{\delta}$ in a practical feedback loop leading to nearly null feedback force, i.e., $\bar{u}_{SD} \rightarrow 0$. That is, the SD-DDR functions as a passive absorber. A remedy is to increase the branch number k so that $\bar{\tau}_{1,2}^{[1]} = 79.3\text{ms} > \bar{\delta}$, which, however, destabilizes the coupled system, as demonstrated in Fig. 10(a).

On the other hand, we have $(\bar{g}^{[2]}, \bar{\tau}_{1,2}^{[2]}) = (-51.58\text{kg} \cdot \text{s}^{-1}, 76.5\text{ms})$ for the tuned MD-DDR when $\bar{\tau}_2 = \bar{\delta}$. Note that $k = 2$ is selected for

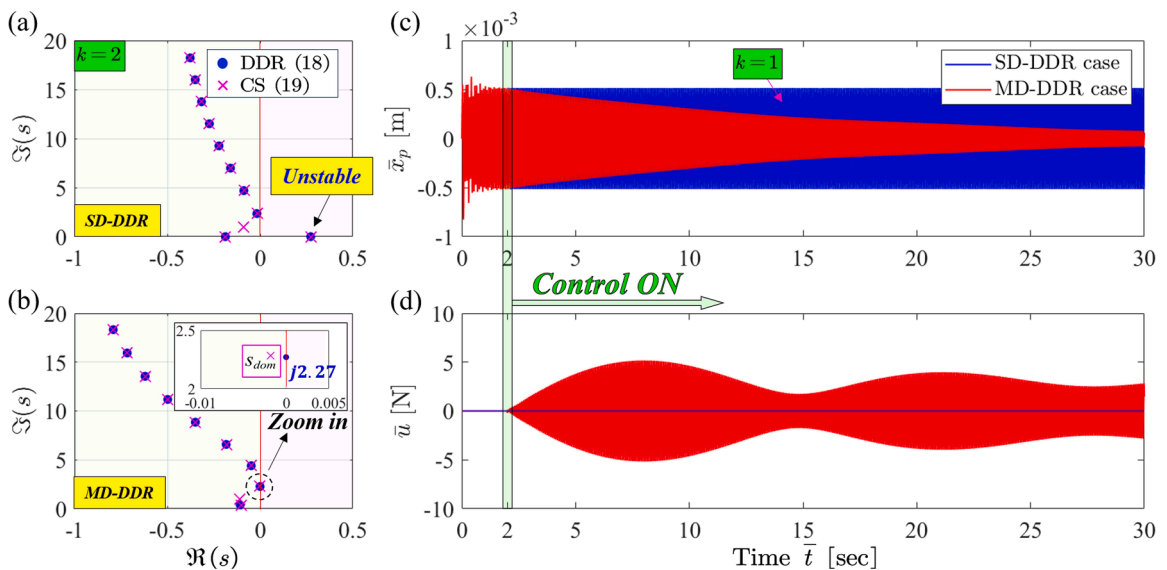


Fig. 10. (a) and (b) represent the spectra in the SD-DDR and the MD-DDR cases, respectively. (c) and (d) depict the dynamics of the primary structure and the feedback forces, respectively. Feedback actuation is activated at $\bar{t} = 2\text{sec}$.

the smallest positive tuned delay to satisfy $\bar{\tau}_{1,k}^{[2]} > \bar{\tau}_2$. Indeed, the required control parameters of the MD-DDR are achievable by hardware, whereas the frequency $\omega = 2.27$ lies in the unstable frequency gap of Fig. 5. To this end, we increase $\bar{\tau}_2$ to $2\bar{\delta}$ (i.e., $\tau_2 = 0.2$) leading to $(\bar{g}^{[2]}, \bar{\tau}_{1,2}^{[2]}) = (-19.65\text{kg} \cdot \text{s}^{-1}, 73.8\text{ms})$. The resulting spectra are shown in Fig. 10(b), indicating that the coupled system is stable when the MD-DDR resonates at $\omega = 2.27$ for complete vibration suppression. More intuitively, dynamics of the primary structure corresponding to the SD-DDR tuned with $k = 1$ and the MD-DDR tuned with $k = 2$ are compared in Fig. 10(c).

Clearly, the SD-DDR yields no vibration suppression agreeing with the null feedback force $\bar{u}_{SD} = 0$ shown in Fig. 10(d). In comparison, the MD-DDR still has favorable effects, although a longer transient process than that in Fig. 9 is required, which is related to a smaller spectra abscissa of the dominant root s_{dom} , see Fig. 10(b). Besides, increasing resonator damping ζ_a is known to prolong the tuned delay $\tau_{1,k}^{[1]}$ [28], while we stress that the SD-DDR still performs poorly in the high-frequency band even if we are allowed to tune ζ_a in real-time. From the form of Eq. (20), the damping term ζ_a only appears in the function $\text{atan2}(\cdot)$ which is upper bounded by π , while the decreasing rate of $\tau_{1,k}^{[1]}$ concerning ω is exponential, see Fig. 2 and Fig. 3. Hence, increasing ζ_a to overcome the hardware constraint $\bar{\tau}_{1,k}^{[1]} > \bar{\delta}$ in the high-frequency band yields a tuned delay value around $\bar{\delta}$ at best, leading to a very small feedback force and thus the poor vibration suppression performance as in Fig. 10(c).

7.3. Reversed polarity of the distributed-delayed feedback control

Fig. 9 and Fig. 10 have shown that the performance of the SD-DDR is related to whether the tuned parameter pair $(g^{[1]}, \tau_{1,k}^{[1]})$ is achievable by hardware. Note from Fig. 9 that very effective vibration suppression can be obtained, although it is incomplete. Revisiting Section 4.2, the theoretically required gain $g^{[1]}$ of the SD-DDR could exhibit an opposite polarity to the corrected one $g^{[2]}$, and therefore poor vibration suppression could be resulted in even if the tuned pair $(g^{[1]}, \tau_{1,k}^{[1]})$ is compatible with a practical feedback loop. Given the upper bound $\omega < 1.671$ of the SD-DDR as per Fig. 2, we consider $\omega = 1.7$ (i.e., $\bar{\omega} = 9.72\text{Hz}$) for demonstration such that $(\bar{g}^{[1]}, \bar{\tau}_{1,1}^{[1]}) = (25.02\text{kg} \cdot \text{s}^{-1}, 5.2\text{ms})$, leading to Fig. 11.

From Fig. 11(a), the rightmost root of the SD-DDR subsystem is far from the imaginary axis, thus yielding no noticeable suppression as verified in Fig. 11(c). Furthermore, the motion amplitude of the primary structure is even amplified once the feedback actuation is activated. That is, the SD-DDR plays a role opposite to its original intentions. Note that the feedback loop now precisely performs the designated control parameters, and thus such counter-intuitive results can be inexplicable except for the real reason: the ignored effect of loop delay $\bar{\delta}$ on the distributed delayed control logic. Alternatively, we select $\tau_2 = 0.3$ for MD-DDR to take $\bar{\delta}$ into account and to lie the $\omega = 1.7$ within the stable regions of Fig. 5, yielding the corrected tuned parameter pair $(\bar{g}^{[2]}, \bar{\tau}_{1,2}^{[2]}) = (-11.644\text{kg} \cdot \text{s}^{-1}, 99.8\text{ms})$. The required imaginary roots for the resonance of MD-DDR appear in Fig. 11(b), leading to the complete vibration suppression in Fig. 11(c). One should notice that the poor vibration suppression of the SD-DDR in Fig. 11 is attributed to the control logic itself regardless of the operability of the control parameters by hardware, indicating that the loop delay $\bar{\delta}$ can significantly deteriorate the control performance even if it is negligible, a counter-intuitive conclusion.

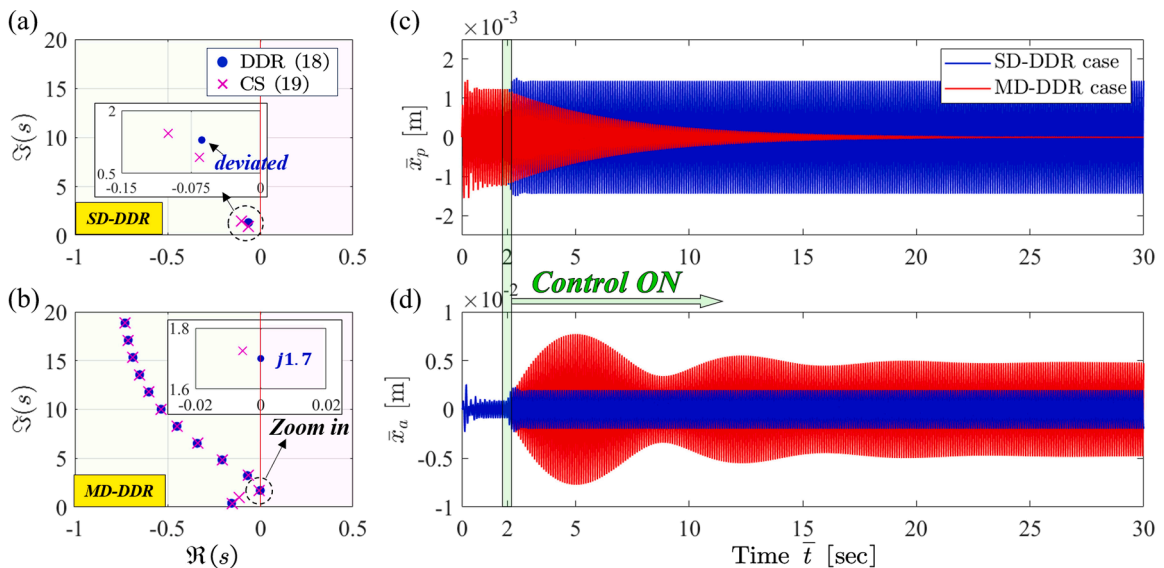


Fig. 11. (a) and (b) represent the spectra in the SD-DDR and MD-DDR cases, respectively. The dynamics of the coupled system when deploying the SD-DDR and MD-DDR are compared in (c) and (d), where the feedback actuation is activated at $\bar{t} = 2\text{sec}$.

7.4. Expedited transient process by tuning τ_2 and numerical implementation of delays

Let us next test the expedited transient process by optimizing τ_2 as mentioned in Section 6, and the vibration frequency $\omega = 1.17$ (i.e., $\bar{\omega} = \omega\bar{\omega}_p = 6.687\text{Hz}$) is considered following Fig. 8. Accordingly, the vibration suppression performance of the MD-DDR tuned with the inherent delay $\tau_2 = \delta = 0.1$ and the optimal one $\tau_2 = \tau_{2,opt} = 1.1065$ for the fastest transient process is compared in Fig. 12, and the associated tuned parameter pairs are listed in Table 2.

Spectra of the MD-DDR and the coupled system shown in Fig. 12(a) and (b) indicate that MD-DDR tuned with both τ_2 values can yield the expected complete vibration suppression in steady states. However, distributions of the dominant root s_{dom} in such two cases are different, leading to different transient behaviors. From Fig. 12(b), we have $\Re(s_{dom}) = -0.044$ and $\Re(s_{dom}) = -0.069$ for $\tau_2 = \delta$ and $\tau_2 = \tau_{2,opt}$, respectively, yielding the associated settling time as $\bar{t}_s = 2.51\text{sec}$ and $\bar{t}_{s,opt} = 1.61\text{sec}$ as per Eq. (47). The corresponding motions of the primary structure are shown in the interval $\bar{t} \in [6\text{sec}, 10\text{sec}]$ of Fig. 12(c) and (d), where theoretical settling time agrees well with numerical results, and the expedited transient process by tuning $\tau_2 = \tau_{2,opt}$ compared with the case $\tau_2 = \delta$ can be clearly found. Hence, compared to the SD-DDR, the MD-DDR not only improves performance in steady states for complete vibration suppression but also yields a faster transient process.

At last, we consider the numerical implementation of the control delays mentioned in Remarks 5 and 6. Due to the existence of the sampling time $\Delta\bar{t}$, the actual output of $(\bar{\tau}_1, \bar{\tau}_2)$ is $(\bar{\tau}_{ACT,1}, \bar{\tau}_{ACT,2})$ as per Eq. (36), results of which are integrated into Table 2. Note that the condition $\bar{\tau}_{ACT,2} = \bar{\tau}_2$ means that numerical implementation cause no errors for $\bar{\tau}_2$ output thanks to the relationship $(\bar{\tau}_2 - \bar{\delta}) / \Delta\bar{t} \in \mathbb{Z}^+ \cup 0$. Then, the completeness of vibration suppression depends on the implementation of the tuned delay $\bar{\tau}_{1,k}^{[2]}$, and it is evaluated in the time interval $\bar{t} \in [6\text{sec}, 10\text{sec}]$ in Fig. 12(c) and (d), where residual vibrations exhibit a favorable smaller amplitude in the case with a larger $\bar{\tau}_{1,k}^{[2]}$, agreeing with Remark 6. This observation provides a guideline for optimizing τ_2 to consider both transient process and numerical implementation of (τ_1, τ_2) , and clearly, the given case $\tau_2 = \tau_{2,opt}$ indicates that such two aspects can simultaneously benefit from the optimization. Comparing Fig. 9, Fig. 11, and Fig. 12, one can conclude that compared to the hardware performance itself, its effects on the control logic deserve more attention when deploying the distributed-delayed control, and clearly, the MD-DDR provides a good solution.

8. Conclusions

This work generalizes the earlier single-delay distributed delayed resonator (SD-DDR) by taking the inevitable loop delay $\bar{\delta}$ inherent in the control system into account, thus creating a so-called MD-DDR. The main aim is to analyze the effects of $\bar{\delta}$ on vibration suppression and how one can treat $\bar{\delta}$ as a tunable parameter to enhance performance, aiming to fully exploit the strength of the distributed-delayed control logic by considering multiple-delay effects and moving this control logic closer to real applications. Based on the same parameters as the actual experimental setup used for SD-DDR studies [36,37], numerous comparisons between the SD-DDR and the proposed MD-DDR are performed, yielding important new findings as follows.

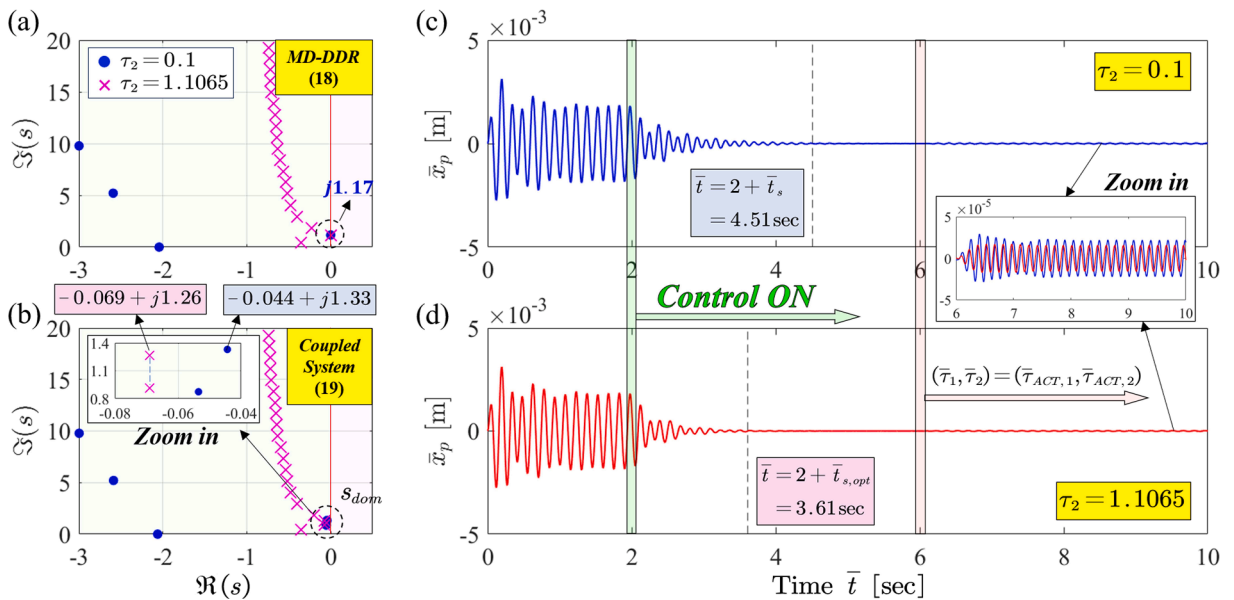


Fig. 12. (a) and (b) represent the spectra of the MD-DDR and the coupled system, respectively. The dynamics of the primary structures in the considered two τ_2 cases are compared in (c) and (d), where feedback actuation is activated at $\bar{t} = 2\text{sec}$.

Table 2

The tuned control parameters of the MD-DDR for $\omega = 1.17$ and $\tau_2 = [0.1, 1.1065]$.

τ_2	$\bar{\tau}_2$	k	$(g^{[2]}, \tau_{1,k}^{[2]})$	$(\bar{g}^{[2]}, \bar{\tau}_{1,k}^{[2]})$	$(\bar{\tau}_{ACT,1}, \bar{\tau}_{ACT,2})$
0.1	2.8 ms	1	(0.0216, 1.415)	(1.181kg · s ⁻¹ , 39.4ms)	(39.8ms, 2.8ms)
1.1065	30.8 ms	2	(-0.0379, 5.779)	(- 2.070kg · s ⁻¹ , 160.9ms)	(160.8ms, 30.8ms)

- Half-angle substitutions [40] make it possible to analytically perform control parameter tuning and complete stability analysis in multiple-delay cases. Hence, the MD-DDR corrects the deviated tuned parameters of the SD-DDR caused by the overlooked effect of loop delay $\bar{\delta}$ on control logic, yielding enhanced vibration suppression.
- Hardware constraint $\bar{\tau}_{1,k}^{[1]} > \bar{\delta}$ greatly limits the operable high-frequency band of the SD-DDR, even if the SD-DDR and the associated coupled system are both stable. Alternatively, the tunable $\bar{\tau}_2$ of the MD-DDR extends both the lower and the upper operable frequency band under the logic constraint $\bar{\tau}_{1,k}^{[2]} > \bar{\tau}_2$.
- Loop delay $\bar{\delta}$ can reverse the polarity of the feedback actuation so that the SD-DDR can counter-intuitively yield no vibration suppression even if $\bar{\delta}$ is negligible and even if the tuned parameter pairs $(\bar{g}^{[1]}, \bar{\tau}_{1,k}^{[1]})$ are precisely achievable by hardware. Remarkably, this is an inherent property of the distributed delayed control logic itself. In comparison, complete vibration suppression by the proposed MD-DDR can be guaranteed as long as the associated tuned parameter composition $(\bar{g}^{[1]}, \bar{\tau}_{1,k}^{[1]}, \bar{\tau}_2)$ is achievable and the coupled system is stable.
- Conventional brute-force seeking procedure for the optimal control parameters generating the fastest transient process, or equivalently the leftmost dominant root s_{dom} of the coupled system, can be simplified. An exclusive optimization procedure by analyzing the special behaviors of the dominant root locus (locus of s_{dom}) is given, yielding exact results at a low enough computational cost. In addition, increasing the loop delay $\bar{\delta}$ by tuning $\bar{\tau}_2$ can reduce the settling time by more than 30%. Note that all benefits of tuning $\bar{\tau}_2$ stem from the distributed-delayed control logic itself.

On the other hand, the negative effects of the deviations of the tuned delay caused by numerical implementation mentioned in Remark 6 are alleviated by increasing the branch number k , see Remark 6 and Section 7.4 The previous study [37] handled this issue by designing an additional filter. As a further step, our future work aims to eradicate such negative effects by modifying the control logic or designing an additional filter (the integral operation itself is already one such operation) while also taking into account the previously overlooked numerical implementation of the tuned gain, or essentially, the final feedback actuation force. More general results will be given by considering the multiple-delay effects, and experimental results will be investigated. As for the exact optimization for the leftmost s_{dom} when no jump phenomenon occurs on the dominant root locus, as mentioned in Remark 8, further discussions are left to another ongoing specific report.

CRedit authorship contribution statement

Yifan Liu: Conceptualization, Methodology, Writing – original draft, Writing – review & editing. **Nejat Olgac:** Methodology, Supervision, Writing – review & editing. **Li Cheng:** Project administration, Supervision, Writing – review & editing.

Declaration of competing interest

The authors declare that they have no known competing financial interests or personal relationships that could have appeared to influence the work reported in this paper.

Data availability

Data will be made available on request.

Appendix A. Construction of integral operation

The integral operation of the distributed logic \bar{u}_{MD} given in Eq. (12) collects all the acceleration information of the MD-DDR within the time interval $\bar{t} \in [\bar{t} - \bar{\tau}_1, \bar{t} - \bar{\tau}_2]$. Considering that the lower bound of the integrator block of Simulink is zero, the required time interval can be obtained by intuitively excluding the interval $\bar{t} \in [0, \bar{t} - \bar{\tau}_1]$ from $\bar{t} \in [0, \bar{t} - \bar{\tau}_2]$. The associated Simulink construction is shown in Fig. 13(a).

Besides, an alternative is given in Fig. 13(b) to accommodate practical situations where measurement noise inevitably exists in the resonator acceleration signals. Note that the two configurations differ in the sequences of performing integration and subtraction. Although they produce the same results when the noise is white, the biased noises can cause registry overflow in the integrator memory when adopting Fig. 13(a). As an alternative, the subtraction operation before the integrator in Fig. 13(b) eliminates the bias effects as long as the two delayed terms use the same discretization points in numerical implementation.

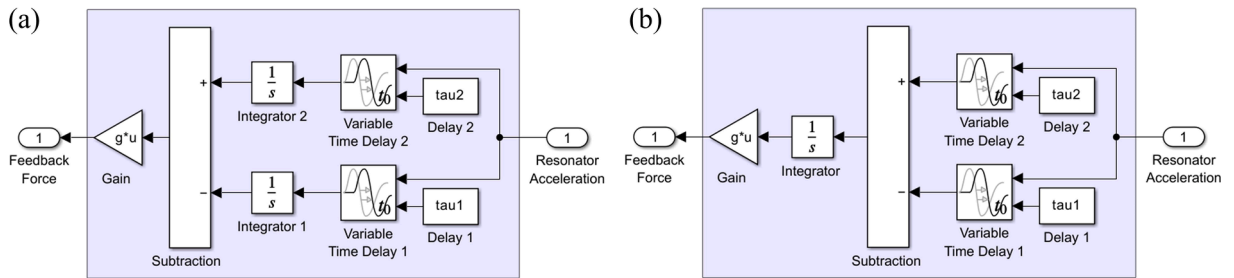


Fig. 13. (a). An intuitive construction of the multiple-delay distributed-delayed logic \bar{u}_{MD} in Simulink. (b). A recommended alternative of (a) for practical applications.

Appendix B. Simulink models and simulation results in Section 7

All Simulink models and simulation results in Section 7 can be found on <https://drive.google.com/drive/folders/1SxKM02NdsKFdbeixgkP3d7xTfvzQiEeK?usp=sharing>.

References

- [1] H. Frahm, Device for damping vibrations of bodies, US patent (1911) 3576–3580.
- [2] J. Den Hartog, J. Ormondroyd, Theory of the dynamic vibration absorber, ASME J. Appl. Mech. 50 (1928) 11–22.
- [3] N. Olgac, B. Holm-Hansen, A novel active vibration absorption technique: delayed resonator, J. Sound Vib. 176 (1994) 93–104.
- [4] T. Vyhldal, N. Olgac, V. Kučera, Delayed resonator with acceleration feedback—Complete stability analysis by spectral methods and vibration absorber design, J. Sound Vib. 333 (2014) 6781–6795.
- [5] S.-M. Kim, M.J. Brennan, Active vibration control using delayed resonant feedback, Smart mater. structures 22 (2013) 095013.
- [6] P.M. Nia, R. Sipahi, Controller design for delay-independent stability of linear time-invariant vibration systems with multiple delays, J. Sound Vib. 332 (2013) 3589–3604.
- [7] Y. Zhang, C. Ren, K. Ma, Z. Xu, P. Zhou, Y. Chen, Effect of delayed resonator on the vibration reduction performance of vehicle active seat suspension, J. Low Frequency Noise, Vib. Active Control 41 (2022) 387–404.
- [8] G. Yan, M. Fang, J. Xu, Analysis and experiment of time-delayed optimal control for vehicle suspension system, J. Sound Vib. 446 (2019) 144–158.
- [9] Y. Sun, J. Xu, Experiments and analysis for a controlled mechanical absorber considering delay effect, J. Sound Vib. 339 (2015) 25–37.
- [10] J. Xu, Y. Sun, Experimental studies on active control of a dynamic system via a time-delayed absorber, Acta Mechanica Sinica 31 (2015) 229–247.
- [11] O. Eris, B. Alikoc, A.F. Ergenc, A new delayed resonator design approach for extended operable frequency range, J. Vib. Acoust. (2018) 140.
- [12] D. Pilbauer, T. Vyhldal, W. Michiels, Optimized design of robust resonator with distributed time-delay, J. Sound Vib. 443 (2019) 576–590.
- [13] C.-X. Liu, Y. Yan, W.-Q. Wang, Resonance and chaos of micro and nano electro mechanical resonators with time delay feedback, Appl. Math. Model. 79 (2020) 469–489.
- [14] C.-X. Liu, Y. Yan, W.-Q. Wang, Resonances and chaos of electrostatically actuated arch micro/nanoresonators with time delay velocity feedback, Chaos, Solitons Fractals 131 (2020) 109512.
- [15] L. Hernández-Villa, D. Melchor-Aguilar, On stability of SDOF systems with delayed position and velocity feedback, J. Vibrat. Control 29 (2023) 3838–3848.
- [16] M. Karama, M. Hamdi, M. Habbad, Energy harvesting in a nonlinear energy sink absorber using delayed resonators, Nonlinear Dyn. 105 (2021) 113–129.
- [17] F. Wang, X. Sun, H. Meng, J. Xu, Time-delayed feedback control design and its application for vibration absorption, IEEE Trans. Industr. Electron. 68 (2020) 8593–8602.
- [18] X. Sun, S. Zhang, J. Xu, Parameter design of a multi-delayed isolator with asymmetrical nonlinearity, Int. J. Mechan. Sci. 138 (2018) 398–408.
- [19] D. Huang, S. Zhou, R. Li, D. Yurchenko, On the analysis of the tristable vibration isolation system with delayed feedback control under parametric excitation, Mech. Syst. Signal Process. 164 (2022) 108207.
- [20] B. Yan, X. Wang, H. Ma, W. Lu, Q. Li, Hybrid time-delayed feedforward and feedback control of lever-type quasi-zero-stiffness vibration isolators, IEEE Trans. Industr. Electron. 99 (2023) 1–10.
- [21] X. Mao, W. Ding, Nonlinear dynamics and optimization of a vibration reduction system with time delay, Commun. Nonlinear Sci. Numer. Simul. 122 (2023) 107220.
- [22] X. Sun, F. Wang, J. Xu, Dynamics and realization of a feedback-controlled nonlinear isolator with variable time delay, J. Vib. Acoust. 141 (2019) 021005.
- [23] N. Olgac, R. Jenkins, Actively tuned noncollocated vibration absorption: an unexplored venue in vibration science and a benchmark problem, IEEE Trans. Control Syst. Technol. 29 (2020) 294–304.
- [24] D. Filipović, D. Schröder, Control of vibrations in multi-mass systems with locally controlled absorbers, Automatica 37 (2001) 213–220.
- [25] H. Silm, M. Kuře, J. Bušek, W. Michiels, T. Vyhldal, Spectral design and experimental validation of noncollocated vibration suppression by a delayed resonator and time-delay controller, IEEE Trans. Control Syst. Technol. (2023).
- [26] A. Saldanha, H. Silm, W. Michiels, T. Vyhldal, An optimization-based algorithm for simultaneous shaping of poles and zeros for non-collocated vibration suppression, IFAC-PapersOnLine 55 (2022) 394–399.
- [27] A. Saldanha, W. Michiels, M. Kuře, J. Bušek, T. Vyhldal, Stability optimization of time-delay systems with zero-location constraints applied to non-collocated vibration suppression, Mech. Syst. Signal Process. 208 (2024) 110886.
- [28] T. Vyhldal, D. Pilbauer, B. Alikoc, W. Michiels, Analysis and design aspects of delayed resonator absorber with position, velocity or acceleration feedback, J. Sound Vib. 459 (2019) 114831.
- [29] J. Cai, Y. Liu, Q. Gao, Y. Chen, Spectrum-based stability analysis for fractional-order delayed resonator with order scheduling, J. Sound Vib. 546 (2023) 117440.
- [30] J. Cai, Q. Gao, Y. Liu, N. Olgac, Control design, analysis, and optimization of fractional-order delayed resonator for complete vibration absorption, J. Sound Vib. 571 (2024) 118083.
- [31] Y. Liu, J. Cai, N. Olgac, Q. Gao, A robust delayed resonator construction using amplifying mechanism, J. Vib. Acoust. 145 (2023) 011010.
- [32] Z. Šika, T. Vyhldal, Z. Neusser, Two-dimensional delayed resonator for entire vibration absorption, J. Sound Vib. 500 (2021) 116010.
- [33] T. Vyhldal, W. Michiels, Z. Neusser, J. Bušek, Z. Šika, Analysis and optimized design of an actively controlled two-dimensional delayed resonator, Mech. Syst. Signal Process. 178 (2022) 109195.

- [34] Z. Šika, J. Krivošej, T. Vyhlídal, Three dimensional delayed resonator of Stewart platform type for entire absorption of fully spatial vibration, *J. Sound Vib.* (2023) 118154.
- [35] M. Valášek, N. Olgac, Z. Neusser, Real-time tunable single-degree of freedom, multiple-frequency vibration absorber, *Mech. Syst. Signal Process.* 133 (2019) 106244.
- [36] D. Pilbauer, T. Vyhlídal, N. Olgac, Delayed resonator with distributed delay in acceleration feedback—Design and experimental verification, *IEEE/ASME Trans. Mechatron.* 21 (2016) 2120–2131.
- [37] V. Kučera, D. Pilbauer, T. Vyhlídal, N. Olgac, Extended delayed resonators—Design and experimental verification, *Mechatronics* 41 (2017) 29–44.
- [38] Q. Gao, J. Cai, P. Firoozy, S. Guo, H. Hong, Z. Long, Dixon resultant theory for stability analysis of distributed delay systems and enhancement of delay robustness, *J. Franklin Inst.* 359 (2022) 6467–6485.
- [39] N. Olgac, A.S. Kammer, Stabilisation of open-loop unstable plants under feedback control with distributed delays, *IET Control Theory Appl.* 8 (2014) 813–820.
- [40] R. Cepeda-Gomez, N. Olgac, Stability of formation control using a consensus protocol under directed communications with two time delays and delay scheduling, *Int. J. Syst. Sci.* 47 (2016) 433–449.
- [41] A. Ukil, V.H. Shah, B. Deck, Fast computation of arctangent functions for embedded applications: a comparative analysis, 2011 IEEE International Symposium on Industrial Electronics, *IEEE* (2011) 1206–1211.
- [42] Q. Gao, A.S. Kammer, U. Zalluhoglu, N. Olgac, Critical effects of the polarity change in delayed states within an LTI dynamics with multiple delays, *IEEE Trans. Automat. Contr.* 60 (2015) 3018–3022.
- [43] V.B. Kolmanovskii, V.R. Nosov, *Stability of Functional Differential Equations*, Elsevier, 1986.
- [44] N. Olgac, R. Sipahi, An exact method for the stability analysis of time-delayed linear time-invariant (LTI) systems, *IEEE Trans. Automat. Contr.* 47 (2002) 793–797.
- [45] T. Vyhlídal, P. Zitek, Mapping based algorithm for large-scale computation of quasi-polynomial zeros, *IEEE Trans. Automat. Contr.* 54 (2009) 171–177.